Cell Metabolism

Resource

Plasma proteomic signature of frailty in 50,506 adults

Graphical abstract

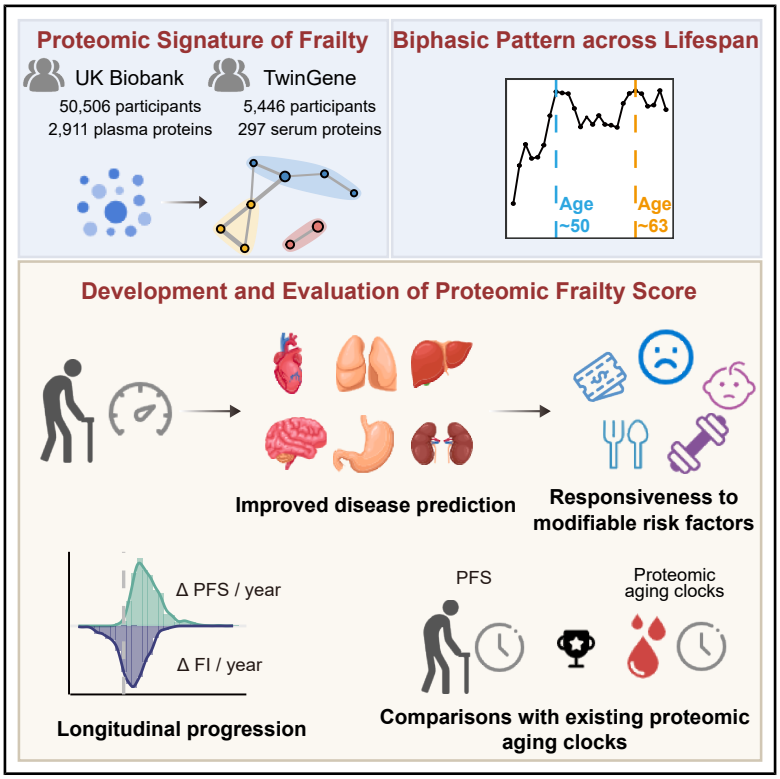

Highlights

- Delineate the most comprehensive plasma proteomic landscape of frailty
- Develop different versions of proteomic frailty scores via the LASSO algorithm
- PFS predicts multiple incident diseases and responds to modifiable factors
- Uncover dynamic changes in frailty-associated proteins across the lifespan

Authors

Xueqing Jia, Weijing Gao, Hampus Hagelin, ..., Emiel O. Hoogendijk, Sara Hägg, Zuyun Liu

Correspondence

huzixin@fudan.edu.cn (Z.H.), sara.hagg@ki.se (S.H.), zuyunliu@zju.edu.cn (Z.L.)

In brief

Jia et al. delineate the most comprehensive plasma proteomic landscape of frailty to date and develop proteomic frailty scores that predict multiple diseases and respond to modifiable risk factors. They identify a biphasic pattern of frailty-related proteomic alterations across the lifespan, revealing critical windows that may inform targeted intervention programs.

Jia et al., 2026, Cell Metabolism *38*, 1–17
May 5, 2026
https://doi.org/10.1016/j.cmet.2026.02.013

CellPress

Please cite this article in press as: Jia et al., Plasma proteomic signature of frailty in 50,506 adults, Cell Metabolism (2026), https://doi.org/10.1016/j.cmet.2026.02.013

Cell Metabolism

CellPress
OPEN ACCESS

Resource

Plasma proteomic signature of frailty in 50,506 adults

Xueqing Jia,[1,15] Weijing Gao,[1,15] Hampus Hagelin,[2,15] Yanjie Zhao,[1] Jingyun Zhang,[1,3] Xingqi Cao,[4] Liming Zhang,[1] Youheng Wu,[1] Lina Ma,[5] Liangkai Chen,[6] Liang Sun,[7] Huan Guo,[8] Cuntai Zhang,[9] Juulia Jylhävä,[2,10,11] Zixin Hu,[12,13,*] Emiel O. Hoogendijk,[14] Sara Hägg,[2,*] and Zuyun Liu[1,16,*]

[1]Second Affiliated Hospital, School of Public Health, Zhejiang Key Laboratory of Intelligent Preventive Medicine, Zhejiang University School of Medicine, Hangzhou, Zhejiang, China
[2]Department of Medical Epidemiology and Biostatistics, Karolinska Institutet, Stockholm, Sweden
[3]Department of Epidemiology and Health Statistics, School of Public Health, Hangzhou Medical College, Hangzhou, Zhejiang, China
[4]Department of General Practice, Sir Run Run Shaw Hospital, Zhejiang University School of Medicine, Hangzhou, Zhejiang, China
[5]Department of Geriatrics, National Research Center for Geriatric Medicine, Xuanwu Hospital, Capital Medical University, Beijing, China
[6]School of Public Health, Tongji Medical College, Huazhong University of Science and Technology, Wuhan, China
[7]The Key Laboratory of Geriatrics, Beijing Institute of Geriatrics, Institute of Geriatric Medicine, Chinese Academy of Medical Sciences, Beijing Hospital/National Center of Gerontology of National Health Commission, Beijing, China
[8]Department of Occupational and Environmental Health, School of Public Health, Tongji Medical College, Huazhong University of Science and Technology, Wuhan, China
[9]Department of Geriatrics, Tongji Hospital, Tongji Medical College, Huazhong University of Science and Technology, Wuhan, China
[10]Faculty of Medicine and Health Technology and Gerontology Research Center (GEREC), Tampere University, Tampere, Finland
[11]Tampere Institute for Advanced Study, Tampere, Finland
[12]Artificial Intelligence Innovation and Incubation Institute, Fudan University, Shanghai, China
[13]Shanghai Academy of Artificial Intelligence for Science, Shanghai, China
[14]Department of Epidemiology & Data Science, Amsterdam Public Health Research Institute, Amsterdam UMC-location VU University Medical Center, Amsterdam, the Netherlands
[15]These authors contributed equally
[16]Lead contact
*Correspondence: huzixin@fudan.edu.cn (Z.H.), sara.hagg@ki.se (S.H.), zuyunliu@zju.edu.cn (Z.L.)
https://doi.org/10.1016/j.cmet.2026.02.013

SUMMARY

Proteomics enables the systematic elucidation of biological mechanisms underlying frailty. Through a large proteome-wide association study of 2,911 plasma proteins from 50,506 UK Biobank participants, we identified 1,339 proteins significantly associated with frailty, highlighting collagen-containing extracellular matrix and vesicle lumen pathways. Replication in the TwinGene study confirmed partial but consistent associations. Mendelian randomization analyses identified five potentially causal proteins for frailty. Moreover, we developed a proteomic frailty score (PFS) that showed strong predictive performance for 199 incident diseases across 13 categories and broad responsiveness to 84 modifiable risk factors. Longitudinal analyses revealed accelerated PFS progression with advancing age and increasing baseline frailty severity. An online tool (https://zipoa.shinyapps.io/frailty/) was created for public PFS calculation. Finally, we observed a biphasic pattern of frailty-associated proteomic dysregulation across the lifespan, with peaks at ages ~50 and ~63. Together, we establish PFS as a biomarker of biological aging while identifying critical windows and molecular targets for frailty interventions.

INTRODUCTION

Frailty is an escalating global public health challenge, characterized by multisystem physiological decline and increased vulnerability to stressors, driving adverse health outcomes and imposing substantial healthcare burdens worldwide.[1,2] Despite decades of research, no globally standardized frailty assessment tool exists.[2] Current approaches, including the widely adopted frailty phenotype[3] and frailty index (FI),[4] predominantly rely on questionnaires, performance-based tests, or routine clinical data. These methods typically require specialized equipment and trained personnel for accurate administration while also exhibiting limitations, including inconsistent validation, restricted scalability, and uncertain capacity to track frailty progression over time,[2] underscoring a critical gap in clinical applicability. Moreover, although efforts have been directed toward biomarker discovery for frailty (e.g., inflammatory indicators, oxidative stress markers, and metabolic profiles),[5–7] the molecular

Please cite this article in press as: Jia et al., Plasma proteomic signature of frailty in 50,506 adults, Cell Metabolism (2026), https://doi.org/10.1016/j.cmet.2026.02.013

mechanisms driving frailty remain poorly elucidated, impeding the development of preventive programs and targeted intervention in the context of rapid population aging.

Proteomics offers a remarkable opportunity to systematically interrogate the protein profiles of health states, facilitating mechanistic understanding and biomarker identification and providing unprecedented insights to inform preventive strategies and advance personalized interventions.[8,9] However, existing proteomic studies on frailty often have small sample sizes (typically in the hundreds to low thousands) or limited proteome coverage.[10–12] Furthermore, observational study designs are inherently limited by residual confounding and reverse causality,[13] complicating the distinction between causal proteins and merely frailty-associated byproducts. Expanding proteome-wide association studies (PWASs) to larger cohorts, integrated with causal inference methodologies, holds promise for advancing our understanding of the biological basis of frailty. Moreover, while previous studies have revealed peripheral proteins associated with aging, the dynamic changes in frailty-specific plasma proteomes during aging remain unknown. Bridging this knowledge gap may pinpoint critical frailty progression phases, enabling timely preventive strategies and mechanistically targeted interventions.

Here, leveraging large-scale proteomic data from the UK Biobank (UKB), we first characterized the proteomic signatures of frailty (manipulated by FI) and elucidated its in-depth biological mechanisms. We then estimated the potential causal relationships between identified proteins and frailty through Mendelian randomization (MR) analyses. Next, we developed a novel proteome-based frailty assessment tool, termed the "proteomic frailty score" (PFS), and evaluated its predictive performance for 655 incident diseases across 13 categories, as well as its responsiveness to 99 modifiable risk factors across six categories. Furthermore, we derived a parsimonious model using a stable reduced set of proteins that retained performance comparable to that of the full model, enhancing its translational potential. To facilitate clinical utility, we also created a publicly accessible online tool for PFS calculation (https://zipoa.shinyapps.io/frailty/). Finally, applying differential expression-sliding window analysis (DE-SWAN), we identified two critical transition points in the frailty-associated proteome during aging. Validation of protein- and pathway-level associations and mortality prediction of the PFS in an independent cohort—the TwinGene study—demonstrated the robustness of our findings. An overview of the study design is shown in Figure 1.

RESULTS

Systemic plasma proteomic alterations underlie frailty

To identify proteins associated with frailty, we conducted PWAS using linear regression on 2,911 plasma proteins in 50,506 UKB participants (participant selection in Figure S1; demographic characteristics in Table S1), with FI (constructed by 39 items) as a continuous outcome. After adjusting for multiple covariates (model 2), 1,339 proteins showed significant associations with 1-standard deviation (SD) FI increase (Figure 2A) at the Bonferroni-corrected threshold ($p < 0.05/2{,}911 = 1.7 \times 10^{-5}$). Notably, 90.2% of these identified proteins exhibited positive associations, suggesting that elevated protein abundance may contribute to or reflect frailty pathophysiology (Figure S2A). Similar results were observed when frailty was treated as a dichotomous variable (non-frail, FI $\leq$ 0.21; frail, FI > 0.21[14]; Figures S2B and S2C). The proteomic association patterns remained robust in analyses specifically performed in (1) participants with complete data on all FI items (n = 41,821; Figure S2D), (2) the randomly selected subset that remains highly representative of the overall UKB participants[15] (n = 43,455; Figure S2E), and (3) the Caucasian (n = 42,406; Figure S2F) and non-Caucasian (n = 8,100; Figure S2G) subgroups. These findings showed high correlations with those from the full sample (all r > 0.9, $p < 2.2 \times 10^{-16}$; Figures S2H–S2K). Linear models incorporating protein × age or protein × sex interaction terms revealed significant interactions for 167 proteins with age and 16 proteins with sex ($p < 0.05/1{,}339 = 3.7 \times 10^{-5}$; Table S2). Detailed PWAS results stratified by age groups (younger, <60 years, n = 27,867; older, ≥60 years, n = 22,639) and sex (males, n = 23,262; females, n = 27,244) are illustrated in Figure S3.

Considering that difficulty engaging in physical activity may be intrinsic to frailty pathophysiology, we repeated the PWAS, excluding regular exercise from model 2. The results remained highly consistent (r > 0.9, $p < 2.2 \times 10^{-16}$), with 1,372 proteins reaching Bonferroni significance, of which 1,333 overlapped with those identified in the original model 2 (Figures S4A and S4B). We further quantified the influence of individual covariates on protein effect sizes compared with model 1 (STAR Methods), observing that body mass index (BMI) had the largest impact, with an average attenuation of 37.1%, while other covariates showed more modest effects (ranging from 2.8% for healthy diet to 9.9% for Townsend deprivation index [TDI]; Figures S4C and S4D). Full results are provided in Data S1.

To further elucidate the biological functions of proteins associated with frailty, we investigated their involvement in functional pathways. Following false discovery rate (FDR) correction, several immune-related pathways emerged as the most significantly enriched, such as leukocyte migration, cytokine-cytokine receptor interactions, and neutrophil degranulation (Figure 2B). These findings align with prior studies emphasizing immune dysregulation in frailty pathophysiology.[16] Using the approach proposed by Shen et al.[17] (STAR Methods), we further eliminated redundant pathways and delineated distinct functional modules associated with frailty. Beyond previously reported modules, such as those related to immune-inflammatory processes,[11,12] we uncovered several novel functional modules. For instance, we identified a module characterized by collagen-containing extracellular matrix (adjusted $p = 1.64 \times 10^{-6}$) and vesicle lumen (adjusted $p = 6.36 \times 10^{-7}$) (Figure 2C).

To elucidate organ-specific expression patterns of proteins associated with frailty, we conducted an enrichment analysis using the putative organ-specific plasma proteome encompassing 18 organ systems[18] (STAR Methods). Among the 1,339 frailty-associated proteins identified above, only 323 (24.1%) were classified as organ specific, directly supporting the notion that frailty is a systemic condition characterized by multisystem dysregulation.[1] These 323 proteins exhibited significant enrichment in 11 organs after FDR correction, particularly in the liver and gastrointestinal system (e.g., stomach, intestine, and pancreas), whereas no significant enrichment was observed in tissues such as the heart, immune system, or kidneys (Figure 2D). These findings suggest that certain organs may play distinct roles in the pathophysiology of frailty. Specifically, the pronounced enrichment

Please cite this article in press as: Jia et al., Plasma proteomic signature of frailty in 50,506 adults, Cell Metabolism (2026), https://doi.org/10.1016/j.cmet.2026.02.013

CellPress
OPEN ACCESS

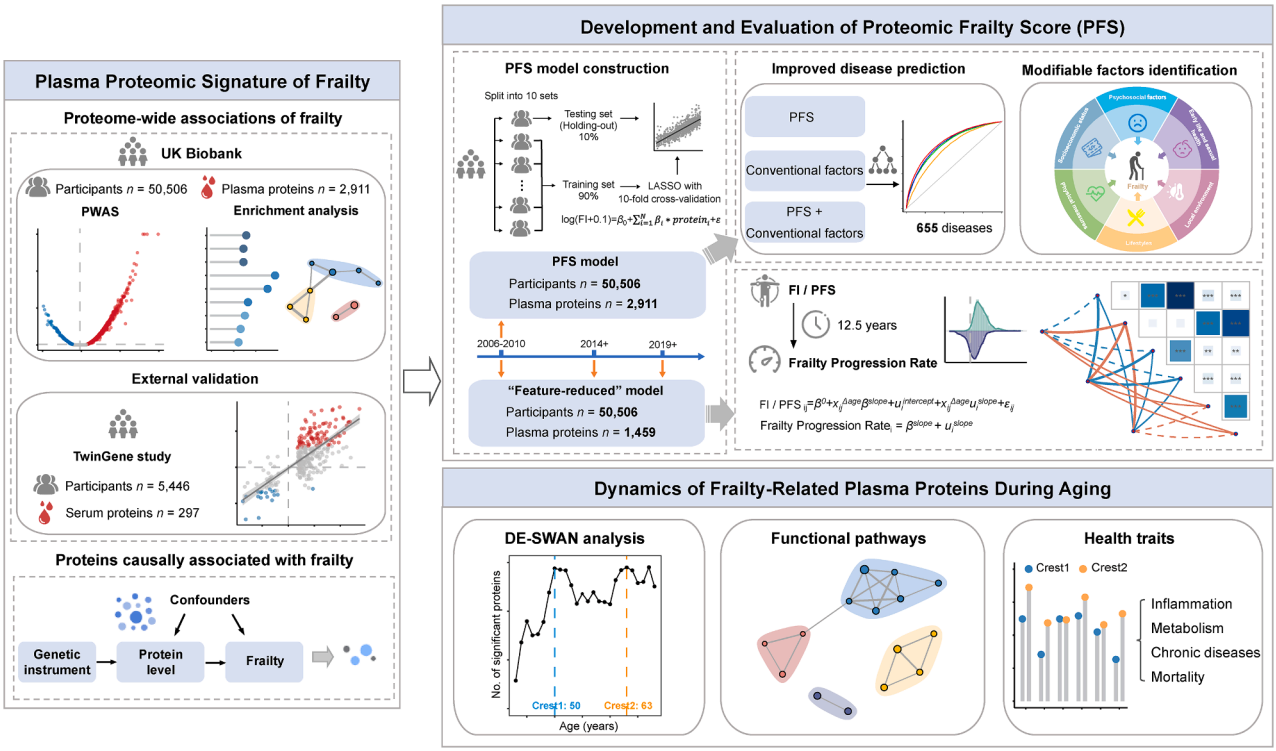

Figure 1. Roadmap of the study

Left: we used the plasma proteomic data of 50,506 UK Biobank (UKB) participants to conduct a proteome-wide association analysis study (PWAS) of frailty (manipulated by frailty index [FI]) and further elucidate the biological functions of frailty-associated proteins. We validated our PWAS findings in an independent external cohort with 5,446 participants (TwinGene study). Next, we performed a proteome-wide two-sample Mendelian randomization (MR) analysis for significant protein-frailty associations to identify proteins with causal roles in frailty. Top right: the development and evaluation of the proteomic frailty score (PFS) model. First, we developed PFS (a full model and a parsimonious model) by applying a nested 10-fold iterative scheme of the LASSO algorithm with 10-fold cross-validation. Then we evaluated the predictive performance of PFS for multiple health-related outcomes and compared it with the conventional factor-based model, as well as their integration. We investigated the associations of 99 potentially modifiable factors across six categories from the UKB baseline survey with PFS. For longitudinal analyses, we focused on 1,459 proteins with <20% missingness across all three visits (baseline, third, and fourth) and retrained a "feature-reduced" PFS model using these proteins. We then estimated the PFS (and FI) change rate for 784 participants with quality-controlled longitudinal proteomic data and complete follow-up time information. We evaluated associations of PFS (and FI) change rate with baseline age, frailty severity, and accumulated disease counts. Bottom right: we performed a differential expression-sliding window analysis (DE-SWAN) to characterize changes in FI-associated proteins across the lifespan, identifying two peaks around ages 50 and 63. Functional enrichment analyses were conducted for crest-specific proteins, and we tested associations between these proteins and health-related traits.

observed in the liver and gastrointestinal system may reflect their central roles in metabolic regulation, detoxification, and nutrient absorption during frailty progression.

Proteomic associations with frailty validated in the TwinGene study

To validate our PWAS findings, we replicated the analysis in an independent external cohort—the TwinGene study—which included 5,446 participants (mean age, 64.33 years) with serum samples (STAR Methods; Table S3). Of the 1,339 frailty-associated proteins identified in the UKB, only 297 were measured in the TwinGene study and were thus available for replication. Despite this limited overlap, we observed similar associations between these 297 proteins and FI across both cohorts (Pearson's r = 0.72; Figure 2E). Among these proteins, 142 (47.8%) exhibited nominal significance, while 109 (36.7%) remained significant after FDR correction (FDR < 0.05), with 108 showing directionally consistent effects compared with those in the UKB. These results may be partly attributed to the relatively small sample size of the TwinGene study, differences in participant characteristics (participants in the TwinGene study were on average over 5 years older than those in the UKB), as well as variations in sample type (serum vs. plasma) and assay methodology (STAR Methods).

Furthermore, we investigated the functional pathways enriched among these replicated proteins and found that several key pathways previously highlighted in the UKB analysis, such as collagen-containing extracellular matrix and cytokine-cytokine receptor interactions, remained significantly enriched (Figure 2F). This cross-cohort consistency supports the robustness of our pathway-level findings and further highlights their biological relevance in frailty pathophysiology.

Proteome-wide MR analyses suggest PYY as a potential causal protein of frailty

To identify proteins exerting potential causal effects on frailty, we performed proteome-wide two-sample MR analyses for significant protein-frailty associations utilizing *cis*-protein quantitative trait loci (*cis*-pQTL) data[15] and genome-wide association study

Please cite this article in press as: Jia et al., Plasma proteomic signature of frailty in 50,506 adults, Cell Metabolism (2026), https://doi.org/10.1016/j.cmet.2026.02.013

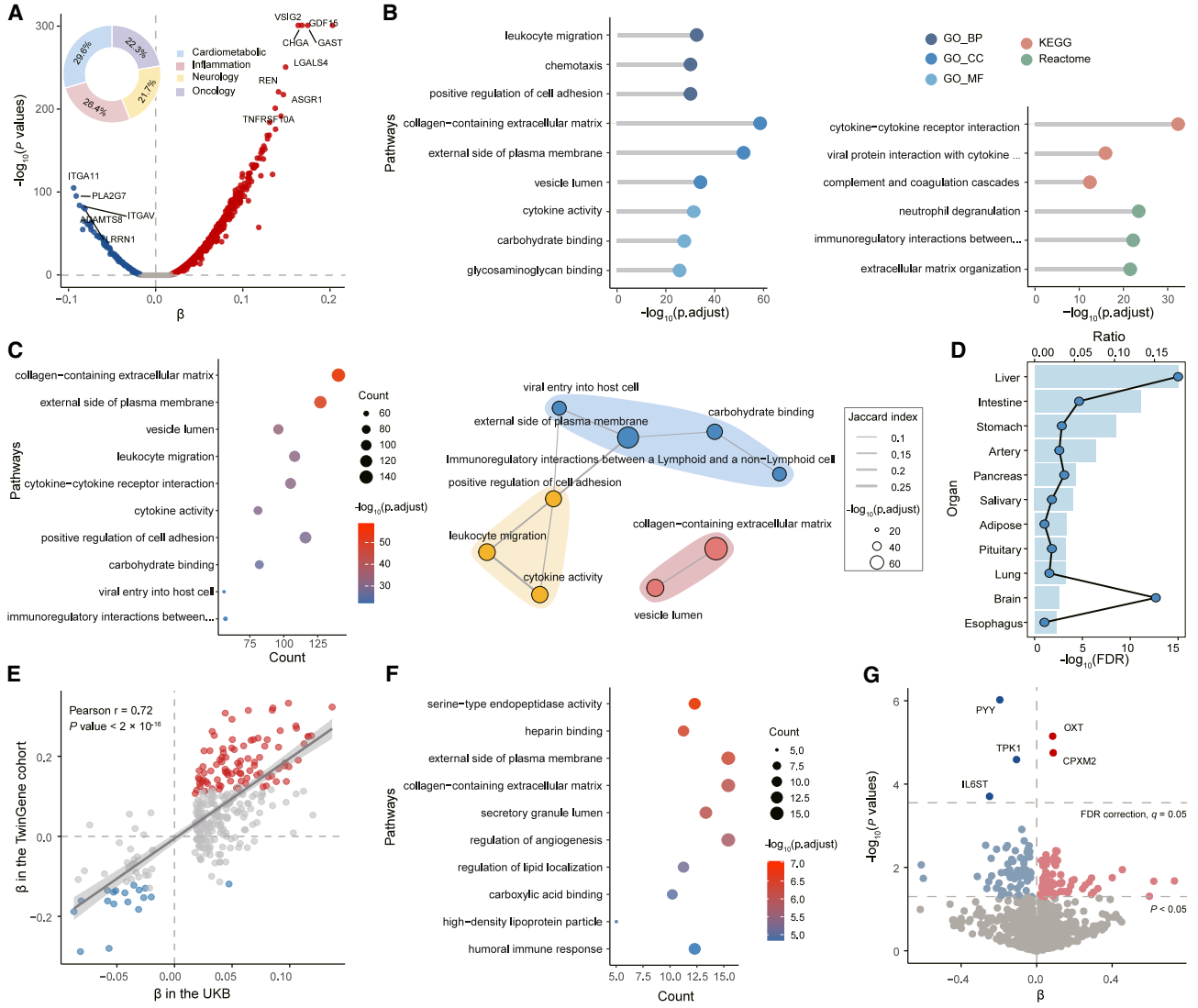

Figure 2. Plasma proteomic profiles of frailty

(A) Volcano plot showing associations between 2,911 plasma proteins and frailty in the UKB (model 2; STAR Methods). The *x* axis represents β coefficients, and the *y* axis represents $-\log_{10}(p$ values). The dashed line indicates the Bonferroni-corrected threshold ($p < 0.05/2{,}911 = 1.7 \times 10^{-5}$). The pie chart depicts the proportions of identified proteins across four panels.

(B) Top three enriched Gene Ontology terms and Kyoto Encyclopedia of Genes and Genomes (KEGG)/Reactome pathways for frailty-associated proteins. BP, biological process; CC, cellular component; MF, molecular function.

(C) Functional module analysis for frailty-associated proteins. Left: top ten representative pathways after eliminating redundant pathways. Right: pathway similarity network.

(D) Enrichment of frailty-associated proteins across 18 organ systems. Only 11 organ systems showing significant enrichment are displayed. Bars indicate $-\log_{10}$(FDR) from Fisher's exact test. Dots represent the ratios of frailty-associated proteins specific to an organ relative to the total number of organ-specific proteins.

(E) Scatterplot showing the correlation of β coefficients for 297 frailty-associated proteins between UKB and the TwinGene study. The Pearson correlation coefficient (r) and corresponding *p* value are shown in the top left. Red dots represent proteins significantly positively associated with frailty, while blue dots represent proteins significantly negatively associated with frailty in the TwinGene study after FDR correction.

(F) Top ten representative pathways for frailty-associated proteins identified in the TwinGene study after eliminating redundant pathways.

(G) Causal associations from a proteome-wide MR study using Wald ratio or IVW methods. The *x* axis represents the estimated β coefficients, and the *y* axis represents $-\log_{10}(p$ values). Dashed lines indicate nominal significance ($p < 0.05$) and FDR-adjusted significance ($q < 0.05$).

(GWAS) summary statistics for FI[19] (STAR Methods). Among the 1,339 PWAS-significant proteins, 1,134 with available instrumental variables (IVs) were analyzed. Using the Wald ratio or inverse-variance weighted (IVW) method, we identified five proteins significantly associated with frailty after FDR correction, along with an additional 129 proteins showing nominal associations (Figure 2G). Among the five proteins, genetically predicted higher levels of OXT and CPXM2 were positively associated with

Please cite this article in press as: Jia et al., Plasma proteomic signature of frailty in 50,506 adults, Cell Metabolism (2026), https://doi.org/10.1016/j.cmet.2026.02.013

frailty, whereas higher levels of peptide YY (PYY), TPK1, and IL6ST were negatively associated with frailty. No evidence of heterogeneity (Cochran *Q* statistics, all $p > 0.05$) or horizontal pleiotropy (MR-Egger intercept, all $p > 0.05$; MR-PRESSO global pleiotropy test, all $p > 0.05$) among the IVs was detected (Tables S4A and S4B).

Furthermore, to evaluate whether the observed protein-FI associations were driven by shared causal variants, we performed colocalization analyses for the five protein-FI pairs (STAR Methods). Among them, only PYY exhibited strong colocalization evidence with frailty (PPH4 = 0.758; Figure S5; Table S4C). Subsequent summary-data-based MR (SMR) and heterogeneity in dependent instruments (HEIDI) tests further supported this finding, with PYY being the only protein passing the SMR test ($p < 0.01$) (Table S4D). Together, these findings suggest PYY as a potential causal candidate for frailty, although further investigations into the mechanism and the roles of other proteins are needed.

Development and predictive features of the PFS model

We first developed a full PFS model using a nested 10-fold iterative scheme of the least absolute shrinkage and selection operator (LASSO) algorithm with 10-fold cross-validation (STAR Methods; Figures 1 and 3). This procedure generated ten sparse models and produced one hold-out set-derived prediction for each participant. Across folds, the models retained 401 to 502 proteins, with 274 proteins consistently selected in all ten folds (Figure 3A). The full PFS showed moderate predictive performance for FI, with an out-of-sample correlation coefficient of 0.522 (Figure 3B). Consistent with FI, the full PFS was significantly elevated in females (vs. males) and older adults (vs. younger) (both $p < 0.001$; Figures 3C and 3D).

To quantify feature stability, we calculated pairwise Jaccard indices for the sets of selected proteins across all folds (Figure 3E). The mean Jaccard similarity was 0.750, indicating moderate consistency despite the high dimensionality. This result suggested that, although some fold-to-fold variability existed, a stable core of proteins (e.g., the 274 consistently selected) reliably captured the majority of the predictive signal. To further evaluate the relative contribution and redundancy of individual proteins, we performed an iterative LASSO procedure by sequentially removing the strongest protein (i.e., the protein with the highest absolute mean β-coefficient across ten folds) at each iteration (STAR Methods). The mean R^2 across folds decreased gradually as proteins were removed, indicating that predictive information was broadly distributed across multiple, partially redundant proteins rather than dominated by a few strong predictors (Figure 3F). Notably, most top-ranked proteins belonged to the 274 consistently selected proteins, reinforcing their robust contributions.

Building on this insight, we applied recursive feature elimination (RFE) using SHAP values to the 274 consistently selected proteins in the full PFS to derive a more parsimonious and interpretable model (STAR Methods). This approach resulted in a core set of 93 proteins and a corresponding simplified PFS model (PFS93), which retained 95% of the predictive performance of the full model ($R^2 = 0.272$; Figures 3G and 3H). In models with fewer than 93 proteins, performance dropped precipitously (Figure 3G). With reduced dimensionality and minimal performance loss, PFS93 has the potential to serve as a more practical alternative to the full PFS. To facilitate public use, we provided an illustrative online tool (https://zipoa.shinyapps.io/frailty/) that allows computation of both the full PFS and PFS93.

PFS outperforms in predicting health-related outcomes

We evaluated the predictive performance of PFS93 (and the full PFS) for health-related outcomes (i.e., all-cause mortality, cause-specific mortality, and 655 incident diseases) and compared it with conventional factor-based models, as well as their integration (Figure 4A and Table S5A for PFS93; Table S5B and Data S1 for the full PFS). PFS93 demonstrated strong predictive capability for all-cause mortality (C-index = 0.710) and cause-specific mortality (e.g., cardiovascular disease [CVD]-related death: C-index = 0.765). Additionally, PFS93 achieved a C-index exceeding 0.70 for 198 incident diseases (30.2% = 198/655) across 13 disease categories. Notably, PFS93 achieved excellent predictions (C-index > 0.8) for 29 diseases, particularly in endocrine, nutritional, and metabolic ($n = 7$ out of 42) and circulatory ($n = 8$ out of 65) diseases, such as type 2 diabetes with peripheral circulatory complications (C-index = 0.936; 95% confidence interval [CI]: 0.916, 0.956) and hypertensive renal disease (C-index = 0.907; 95% CI: 0.888, 0.927). PFS93 significantly outperformed the conventional factor-based model in predicting 115 diseases (17.6% = 115/655), such as diabetic neuropathy (PFS93, C-index = 0.705; conventional factor model, C-index = 0.603, $p < 0.05$). Furthermore, integrating PFS93 with conventional factors significantly improved predictive accuracy for 498 diseases (76.0% = 498/655) (Table S5A).

PFS93 also demonstrated significantly better predictive performance than FI for 296 incident diseases (45.2% = 296/655) across 13 disease categories, particularly in circulatory ($n = 57$ out of 65) and endocrine, nutritional, and metabolic ($n = 37$ out of 42) diseases. When integrated with conventional factors, models incorporating PFS93 continued to outperform those incorporating FI for 169 diseases. By contrast, FI demonstrated significantly better predictive performance than PFS93 for 55 incident diseases (8.4% = 55/655) across seven disease categories, particularly in diseases of the musculoskeletal system and connective tissue ($n = 22$ out of 96) and mental and behavioral disorders ($n = 5$ out of 24). Furthermore, combining PFS93 with conventional factors and FI further improved predictive accuracy compared with models including only conventional factors and FI, with significant enhancements observed for 398 diseases (60.8% = 398/655) (Table S5A). These findings suggest that PFS93 captures additional predictive information not encompassed by FI.

Notably, the performance of PFS93 closely mirrored that of the full PFS model, with only marginal differences across outcomes—slightly stronger for 45 diseases and weaker for 63 diseases (Figure 4B). This reinforces the potential of the parsimonious 93-protein signature as a clinically translatable alternative.

To assess the generalizability of PFS, we constructed a restricted model in UKB using 351 proteins measured by Olink in both UKB and TwinGene, as we did for the full PFS above. Finally, 94 proteins were consistently retained in the restricted model, and their mean β coefficients across ten folds were similar to those for the full PFS (Figure 4C). As expected, the restricted PFS showed reduced performance in UKB relative to the full model due to the smaller protein set, but it remained significantly associated with FI (Figures 4D and 4E). When

Please cite this article in press as: Jia et al., Plasma proteomic signature of frailty in 50,506 adults, Cell Metabolism (2026), https://doi.org/10.1016/j.cmet.2026.02.013

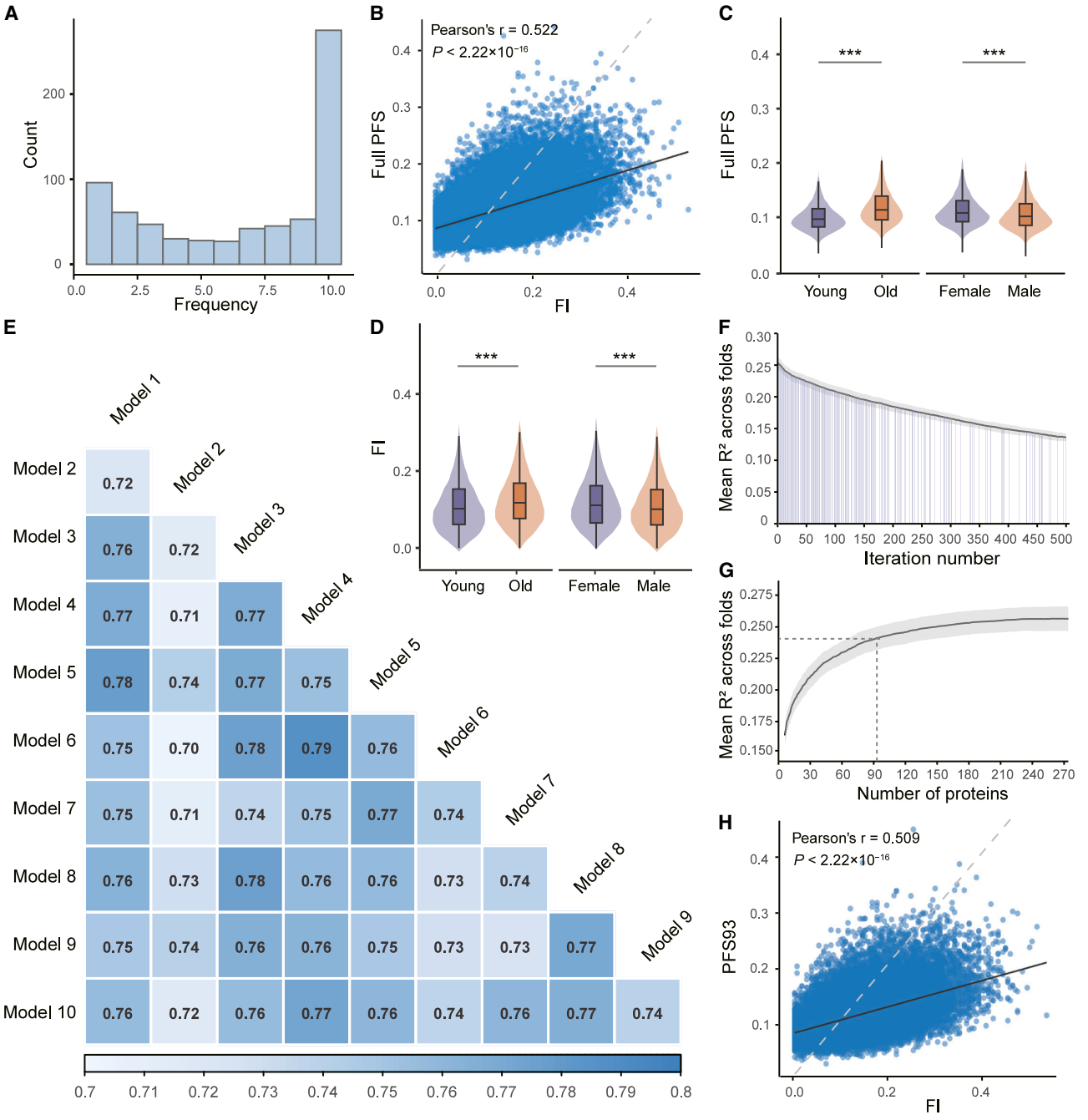

Figure 3. Development and characterization of the PFS and its predictive features

(A) Distribution of protein selection frequencies across the ten folds.

(B) Scatterplot showing the out-of-sample correlation between the full PFS and traditional frailty index (FI) across all participants. Each scatter represents a single participant. The Pearson correlation coefficient (r) and corresponding *p* value are shown in the top left.

(C and D) Violin plots of the full PFS (B) and FI (C) distributions stratified by sex (males, *n* = 23,262; females, *n* = 27,244) and age group (younger, <60 years, *n* = 27,867; older, ≥60 years, *n* = 22,639). ***$p < 0.001$ (two-tailed *t* test).

(E) Heatmap of pairwise Jaccard similarity indices for protein sets selected in each of the ten folds. Higher values indicate greater overlap in feature selection across folds.

(F) Changes in mean out-of-sample R^2 across folds during the iterative LASSO modeling analysis (STAR Methods). Shaded regions indicate iterations in which a protein retained across all folds in the original PFS model was removed.

(G) Changes in mean out-of-sample R^2 across folds during the recursive feature elimination (RFE) analysis based on SHAP values (STAR Methods), identifying a core set of 93 proteins (PFS93) that retained 95% of the predictive performance of the full model.

(H) Scatterplot showing the correlation between the simplified model (PFS93) and the traditional FI across all participants. The Pearson correlation coefficient (r) and corresponding *p* value are shown in the top left.

Please cite this article in press as: Jia et al., Plasma proteomic signature of frailty in 50,506 adults, Cell Metabolism (2026), https://doi.org/10.1016/j.cmet.2026.02.013

CellPress
OPEN ACCESS

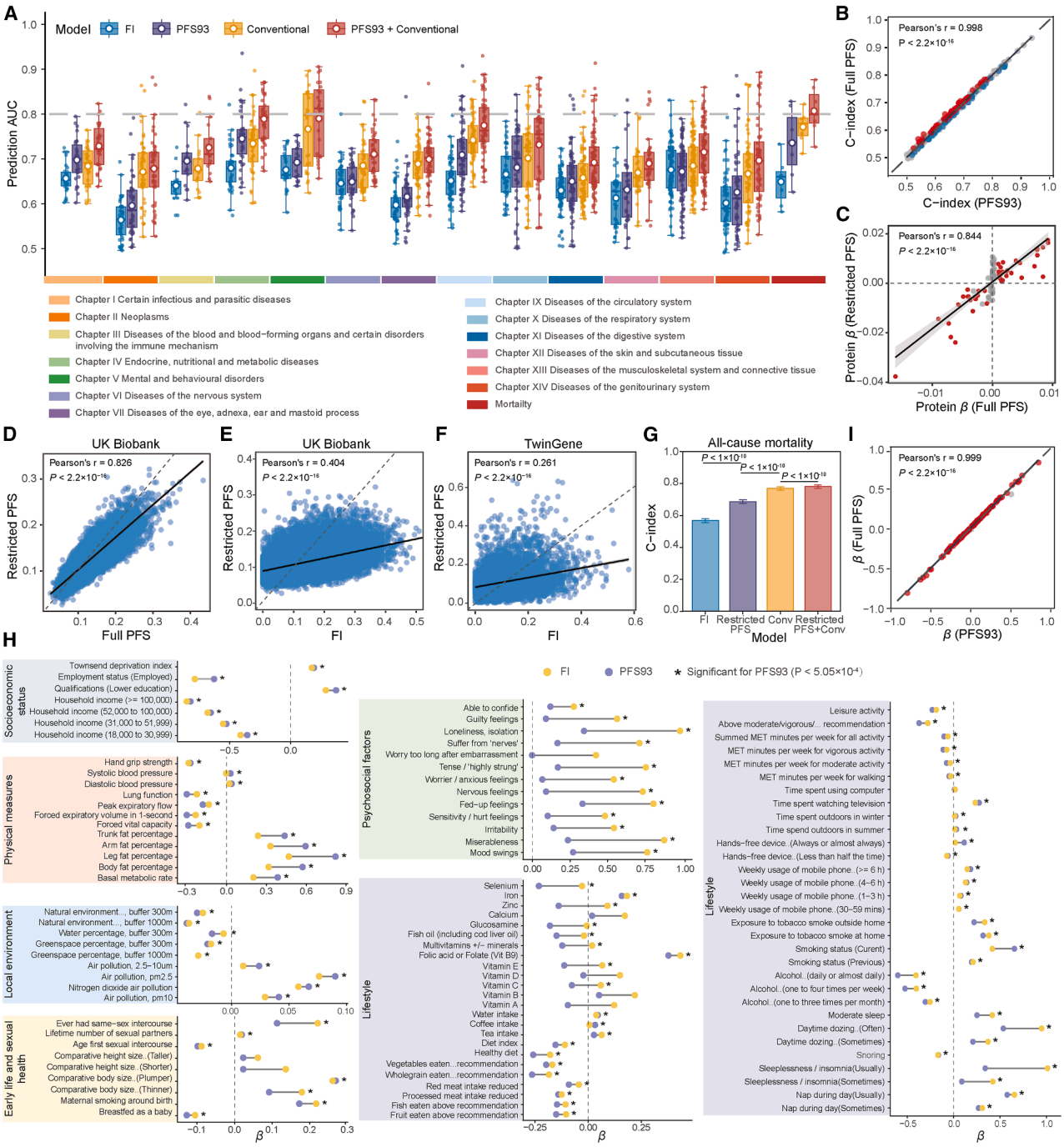

Figure 4. The PFS improves disease prediction and responds to key modifiable risk factors

(A) Discriminative performances (quantified by C-index) for predicting health-related outcomes (i.e., mortality and 655 incident diseases) across four models: the traditional frailty index (FI), the simplified PFS93 (PFS93), the conventional risk factors model, and the PFS93+ conventional risk factors model. Boxplots show the median (line), interquartile range (IQR; box), and whiskers extending to 1.5 × IQR. Hollow circles indicate mean values.

(B) Scatterplot showing the correlation between the C-indices of PFS93 and the full PFS for 655 diseases. Diseases for which PFS93 outperformed the full PFS (n = 45) are in blue, and those performing worse (n = 63) are in red.

(C) Scatterplot showing the correlation between the mean β coefficients of proteins in the restricted and full PFS. Only proteins robustly retained in the restricted PFS were analyzed, and those also robustly retained in the full PFS are highlighted in red.

(D) Scatterplot showing the correlation between the restricted and full PFS across all participants in the UKB.

(E) Scatterplot showing the correlation between the restricted PFS and FI across all participants in the UKB.

(F) Scatterplot showing the correlation between the restricted PFS and FI across all participants in the TwinGene study (n = 6,190).

(legend continued on next page)

Please cite this article in press as: Jia et al., Plasma proteomic signature of frailty in 50,506 adults, Cell Metabolism (2026), https://doi.org/10.1016/j.cmet.2026.02.013

applied to the TwinGene study, the restricted PFS was significantly correlated with FI (Pearson's r = 0.26, $p < 2.2 \times 10^{-16}$; Figure 4F) and retained predictive capacity for all-cause mortality, outperforming FI alone (C-index: 0.687 for restricted PFS vs. 0.568 for FI; Figure 4G). Moreover, combining the restricted PFS with conventional factors yielded a significant improvement in mortality prediction (Figure 4G), supporting the robustness of PFS across independent populations.

PFS broadly responds to modifiable risk factors

We investigated the associations of 99 potentially modifiable risk factors from the UKB baseline survey with frailty, as measured by PFS93 (and the full PFS) and FI. After Bonferroni correction, 83 out of 99 risk factors were significantly associated with PFS93 ($p < 5.05 \times 10^{-4}$; Figure 4H; see Table S6 for the full PFS). Among the top 20 factors, 10 were positively associated with frailty, such as leg fat percentage ($\beta = 0.846$; 95% CI: 0.831, 0.860), smoking status (current vs. never: $\beta = 0.642$; 95% CI: 0.614, 0.669), and TDI ($\beta = 0.189$; 95% CI: 0.181, 0.198), and 10 factors were negatively associated with frailty, such as current employment status (employed vs. unemployed: $\beta = -0.598$; 95% CI: −0.628, −0.569), forced expiratory volume in 1 s ($\beta = -0.298$; 95% CI: −0.309, −0.288), and diet index ($\beta = -0.158$; 95% CI: −0.166, −0.150). A broadly similar exposure-wide association pattern was observed for FI, with most risk factors showing concordant directions of effect. Comparable findings were also noted when stratifying by age and sex (Data S1).

Interestingly, despite the overall similarity, the responses of PFS93 and FI to different categories of modifiable risk factors exhibited notable differences (Figure 4H). For instance, FI showed stronger associations with psychosocial factors (e.g., nervous and worried/anxious feelings) and sleep-related measures (e.g., sleeplessness/insomnia), likely due to its reliance on self-reported psychological and functional status, making it more sensitive to subjective factors. By contrast, PFS93 showed stronger associations with physical measures (e.g., pulmonary function and body composition), dietary quality, and physical activity, which are closely linked to biological changes.

Importantly, analyses based on the PFS93 model yielded nearly identical association profiles to the full PFS (Pearson's r = 0.999 between β estimates; Figure 4I) and recapitulated the same pattern of differences relative to FI (Table S6).

Comparisons with existing proteomic aging studies

We compared proteins consistently retained across all folds in our study with age- or mortality-associated proteins reported in six major published proteomic aging studies (STAR Methods) and observed a moderate overlap. Among the 274 proteins consistently retained in the full PFS model, ten proteins were shared with at least four prior studies—including well-established aging biomarkers such as GDF15, TNFRSF11B, and LTBP2—suggesting that PFS captures a core set of robust and reproducible age-related signals. By contrast, 61 proteins (22.3%) were unique to the full PFS model and absent from all six prior studies, underscoring that PFS captures a partially distinct proteomic signature potentially relevant to physiological decline (Figure 5A). These unique proteins were significantly enriched in immune pathways (e.g., complement and coagulation cascades) as well as pathways related to tissue integrity, repair, and physiological vulnerability (e.g., collagen-containing extracellular matrix, growth factor binding, and axon/neuron development) (Figure 5B). Notably, a similar pattern was observed for the parsimonious PFS93 model: seven proteins (including GDF15) overlapped with at least four prior studies, whereas 17 proteins (18.3%) were unique to PFS93 (Figure 5A). This suggests that, despite its reduced dimensionality, PFS93 preserves conserved aging signals while retaining partially distinctive components related to frailty biology.

Furthermore, we benchmarked the predictive performance of PFS93 (and the full PFS) against three published proteomic aging clocks: an age-based clock from Oh et al.[20] (trained on age) and two clocks from Goeminne et al.[21] (trained on age or all-cause mortality), for health-related outcomes (Figures 5C–5E). PFS93 was significantly correlated with all three clocks (Spearman's r = 0.36–0.57), with stronger correlations than those observed for the FI (Figure 5C). PFS93 significantly outperformed Oh's and Goeminne's age-based clocks for 306 (46.7%) and 333 (50.8%) incident diseases, respectively—particularly for endocrine, nutritional, and metabolic disorders, as well as certain infectious and parasitic diseases. Compared with Goeminne's mortality-based clock, PFS93 showed superior prediction for 120 (18.3%) diseases, particularly those of the musculoskeletal system and connective tissue. Conversely, the published clocks performed better than PFS93 in specific domains: Oh's and Goeminne's age-based clocks outperformed PFS93 in 127 and 112 diseases, respectively—primarily diseases of the eye, adnexa, ear and mastoid process, and neoplasms—while Goeminne's mortality-based clock showed superior prediction for 292 diseases, especially circulatory diseases and neoplasms. However, when integrated with conventional factors, the number of diseases for which the published clocks outperformed PFS93 dropped sharply to just 7 (for Oh's age-based clock), 5 (for Goeminne's age-based clock), and 170 (for Goeminne's mortality-based clock) (Figure 5D). Importantly, adding the PFS93 to models that already contained conventional factors and each of the published clocks further improved prediction accuracy for 461, 473, and 288 diseases, respectively. These findings demonstrate that PFS93 captures biological information complementary to current proteomic aging clocks and enhances their translational utility (Figure 5E).

(G) Discriminative performance (C-index) for all-cause mortality across four models (FI, the restricted PFS, the conventional risk factor model, and the restricted PFS plus conventional risk factors model) in the TwinGene study. Differences in Harrell's C-indices between models were compared using the compareC R package.

(H) Associations of PFS93 and FI with 99 modifiable risk factors across six categories. Linear models were adjusted for age, sex, and ethnicity. Only factors significantly associated with either PFS93 or FI ($p < 0.05/99 = 5.05 \times 10^{-4}$) are shown. Asterisks indicate factors significantly associated with PFS93.

(I) Scatterplot showing the correlation between regression coefficients for the associations of modifiable factors with PFS93 and the full PFS. Factors significantly associated with both PFS93 and the full PFS ($p < 0.05/99 = 5.05 \times 10^{-4}$) are highlighted in red.

Please cite this article in press as: Jia et al., Plasma proteomic signature of frailty in 50,506 adults, Cell Metabolism (2026), https://doi.org/10.1016/j.cmet.2026.02.013

CellPress
OPEN ACCESS

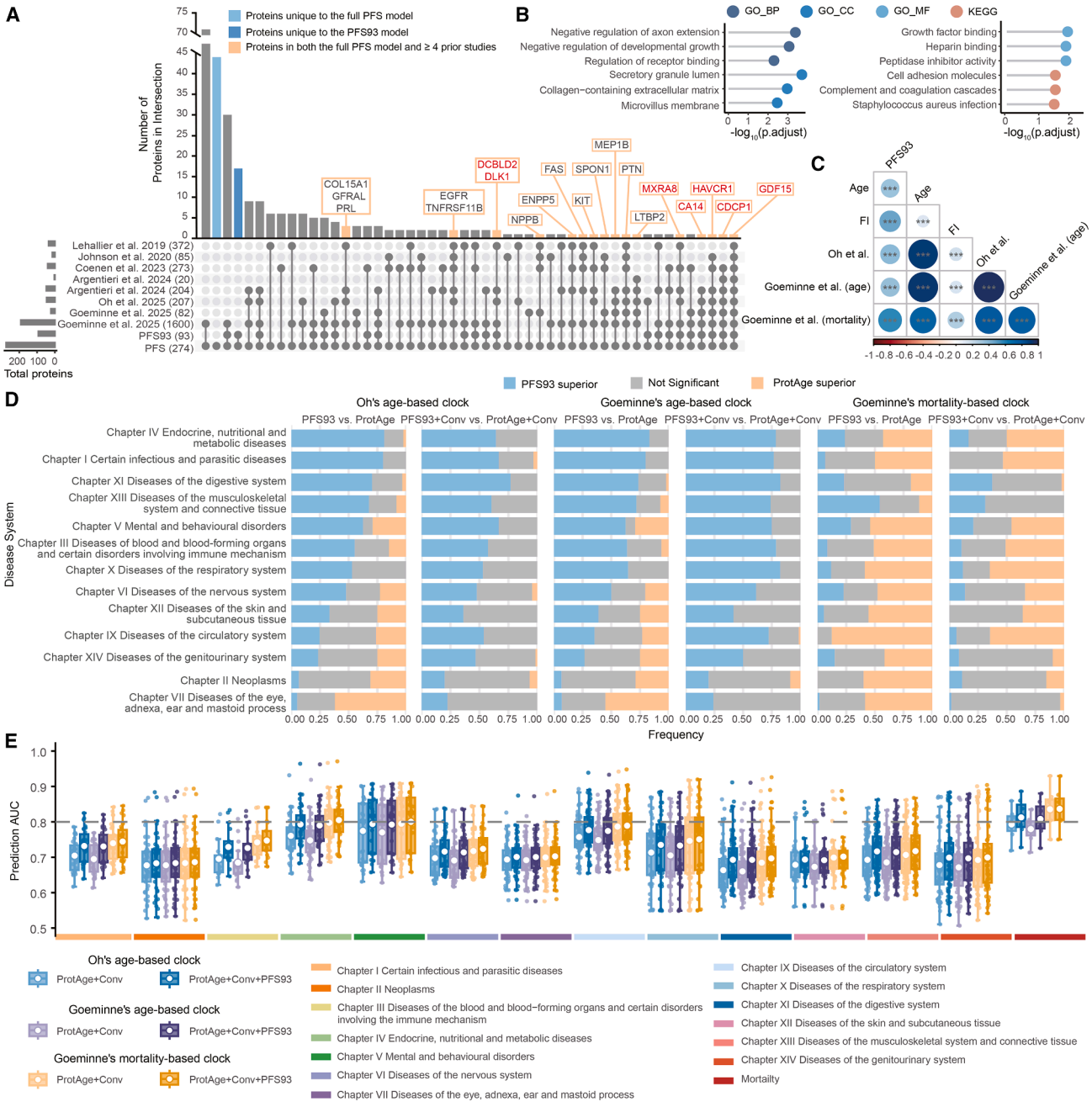

Figure 5. Comparisons of PFS with existing proteomic aging studies

(A) Overlap between proteins consistently retained in the full PFS model (n = 274) and the simplified PFS93 model (PFS93, n = 93) and those reported in six published proteomic aging studies. Proteins highlighted in red are shared between the PFS93 model and at least four prior studies.

(B) Top three enriched Gene Ontology terms and KEGG pathways for 61 proteins unique to the full PFS model. BP, biological process; CC, cellular component; MF, molecular function.

(C) Correlation heatmap between PFS93 and three published proteomic aging clocks: an age-based clock from Oh et al. (trained on age) and two clocks from Goeminne et al. (trained on age or all-cause mortality). Asterisks indicate significance (*p < 0.05, **p < 0.01, ***p < 0.001).

(D) Comparison of predictive performance across disease categories (grouped by ICD-10 chapters), showing the proportion where PFS93 performed better (blue), similarly (gray), or worse (orange) than each proteomic aging clock (ProtAge), either alone or in combination with conventional risk factors.

(E) Discriminative predictive performances (quantified by C-index) for mortality and 655 incident diseases across six models: each proteomic aging clock alone and its combination with PFS93. Boxplots show the median (line), interquartile range (IQR; box), and whiskers extending to 1.5 × IQR. Hollow circles indicate mean values.

Please cite this article in press as: Jia et al., Plasma proteomic signature of frailty in 50,506 adults, Cell Metabolism (2026), https://doi.org/10.1016/j.cmet.2026.02.013

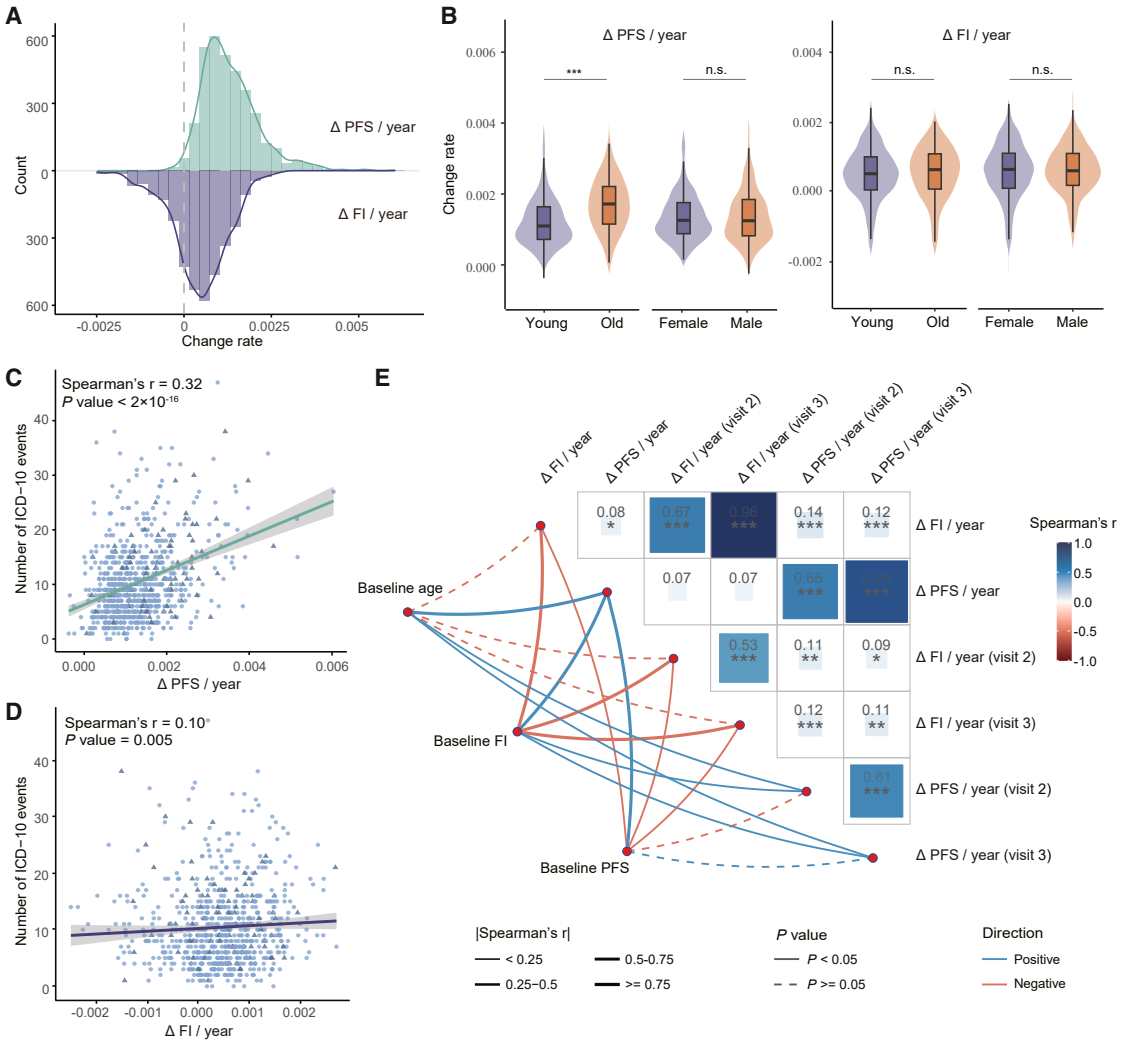

Figure 6. The distinct progression patterns between PFS and traditional FI during aging

(A) Histogram comparing annualized progression rates (Δ/year) of PFS (derived from the "feature-reduced" model) vs. traditional FI. ΔPFS/year and ΔFI/year indicated the frailty progression rate calculated through the mixed-effects model.

(B) Violin plots comparing the distributions of progression rates stratified by sex and age group (<60 vs. ≥60 years). ***$p < 0.001$, two-tailed t test; n.s., not significant ($p \geq 0.05$). Boxplots within violins show the median (center line) and interquartile range (IQR) (box bounds).

(C and D) Scatterplot showing the correlation of the change rates of PFS (C) and traditional FI (D) with the accumulative disease count. Spearman's correlation coefficient (r) and the corresponding p value are shown in the top left.

(E) Heatmap showing the correlations between baseline age, frailty status, and frailty progression pattern. ΔPFS/year and ΔFI/year were calculated as the change from baseline to the third (visit 2) or fourth (visit 3) assessment, divided by the corresponding follow-up time.

Disease-prediction benchmarking analyses for the full PFS model are presented in Figure S6 and Data S1, and the results were broadly consistent with those obtained for PFS93.

Longitudinal PFS changes facilitate sensitive dynamic monitoring of frailty

A subset of ~1,000 participants had proteomic data available at their third and fourth visits in the UKB, enabling us to evaluate frailty progression based on changes in PFS and FI. For longitudinal analyses, we focused on 1,459 proteins with less than 20% missing values across all three visits (baseline, third, and fourth) and retrained the PFS model ("feature-reduced" model) in the 50,506 participants at baseline using these proteins (STAR Methods). The feature-reduced model demonstrated significant correlation with FI ($r = 0.509$, $p < 2.2 \times 10^{-16}$). We then estimated the PFS (and FI) change rate for 784 participants with quality-controlled proteomic data and complete visit-date information across all three visits. As expected, longitudinal analysis revealed frailty progression in most participants (99.1% by PFS; 76.3% by FI) (Figure 6A). Notably, frailty (evaluated by PFS) progressed more rapidly in older adults (≥60 years) compared with younger adults (<60 years) ($p < 0.001$; Figure 6B). Participants with accelerated frailty progression accumulated more diseases, and each 1-SD increase in FI and PFS was associated with an average of 0.6 and 2.5 additional International Classification of Diseases, 10th edition (ICD-10) disease annotations,

Please cite this article in press as: Jia et al., Plasma proteomic signature of frailty in 50,506 adults, Cell Metabolism (2026), https://doi.org/10.1016/j.cmet.2026.02.013

respectively (Figures 6C and 6D). These findings underscore the importance of managing FI progression to mitigate disease burden.

Interestingly, we found that baseline PFS and FI were negatively associated with the change rate of FI but positively associated with the change rate of PFS (Figure 6E). This suggests that FI may be less sensitive in capturing frailty progression, particularly among participants with advanced aging and severe frailty, whereas the PFS demonstrates a unique capacity for dynamically monitoring frailty even in this vulnerable population. These findings remained consistent when using an alternative method to calculate frailty progression rates (subtracting the previous round from the subsequent round and dividing by the follow-up time) (Figure 6E). Our next analysis on the agreement between FI and PFS change rates further supported our hypothesis that PFS may be more sensitive to capturing frailty progression (details in Figure S7; STAR Methods).

Biphasic patterns of frailty-associated proteomic dysregulation across lifespan

Given the undulating nature of the aging plasma proteome, we performed a DE-SWAN analysis to comprehensively characterize changes in frailty-associated proteins across the human lifespan (STAR Methods). We identified two prominent crests occurring around ages 50 and 63, which remained robust across different q value thresholds (Figures 7A and 7B). The proteins associated with these two crests are detailed in Data S1.

To further elucidate the biological functions associated with each crest, we conducted separate functional enrichment analyses for crest-specific proteins (Figure 7C). Proteins from both crests were enriched in shared pathways such as the external side of the plasma membrane but also exhibited crest-specific pathway enrichments, reflecting stage-specific biology. At age 50, proteins were particularly enriched in metabolic and signaling pathways, such as cholesterol metabolism, lipid catabolic processes, carbohydrate derivative catabolic processes, and hormone activity. Whereas proteins associated with the peak at age 63 were particularly enriched in immune-related pathways, such as leukocyte-mediated immunity, cytokine-cytokine receptor interaction, and defense response to bacterium (Figure 7D). These findings indicate that frailty progression with aging is a dynamic, undulating process characterized by waves of changes in plasma proteomes that reflect alterations in underlying biological processes.

We further tested associations between the proteins of two key crests and health-related traits, including diseases and metabolic and inflammatory indicators. We found that proteins at age 50 years showed the most associations with metabolic health traits (e.g., total cholesterol [TC], triglycerides [TGs], and diabetes) and Parkinson's disease, while proteins at age 63 years showed the most associations with multisystem diseases (e.g., dementia, CVD, and cancer) and immune-inflammatory markers (Figures 7E and 7F).

DISCUSSION

This large-scale proteomic analysis of 50,506 UKB participants identified 1,339 plasma proteins significantly associated with frailty, providing unprecedented insights into its proteomic landscape. Through comprehensive functional annotation and MR analyses, we elucidated novel biological pathways implicated in frailty pathogenesis and suggested potential causal roles of several candidate proteins in driving its progression. Replication analyses in the TwinGene study (n = 5,446) confirmed partial but consistent associations at both protein and pathway levels, supporting the reliability of the above findings. Furthermore, we developed a novel proteome-based measure of frailty—the full PFS model, which exhibited robust predictive capacity for a wide spectrum of incident diseases and broad responsiveness to diverse modifiable risk factors, highlighting its potential as a versatile aging biomarker. We also derived a parsimonious model using a stable reduced set of 93 proteins that retained performance comparable to that of the full PFS model, enhancing its translational potential. Longitudinal analyses with three assessments ($n \sim 1{,}000$) revealed an accelerated progression pattern of PFS with advancing age and baseline frailty severity. In addition, we uncovered dynamic changes in frailty-associated proteins across the lifespan, with proteomic alterations peaking at ages 50 and 63, pinpointing critical windows for targeted interventions to mitigate age-related decline.

Previous studies have sought to delineate proteomic biomarkers of frailty in 880 community-dwelling Ashkenazi Jewish older adults (≥65 years)[11] and 3,838 older adults (≥65 years) from the Atherosclerosis Risk in Community (ARIC) study.[12] Building on these, a recent study examined proteomic profiles associated with frailty and mortality in prefrail or frail persons in the UKB[13]—the largest cohort spanning a wider age range to date. Our study extends this work by adopting a continuous FI framework, integrating proteome-wide MR, developing a PFS that substantially broadens outcome prediction beyond mortality in prefrail or frail persons, and leveraging longitudinal and DE-SWAN analyses to capture dynamic proteomic changes and identify potential intervention windows. These advances expand both the biological and translational scope of frailty research.

Complemented by in-depth functional exploration, we confirmed several frailty-associated proteins (e.g., FABP4) and functional pathways consistent with prior research,[11,12] while also identifying novel proteins and pathways potentially involved in frailty development. For example, PYY—a gut-derived hormone secreted by enteroendocrine L cells—emerged as a potential causal biomarker of frailty. Beyond its canonical roles in regulating appetite, energy homeostasis, and gastrointestinal motility, accumulating evidence implicates PYY in age-related metabolic traits (e.g., body weight), musculoskeletal integrity, and inflammatory pathways.[22–25] PYY can also signal to the central nervous system via vagal afferents or direct blood-brain transport, potentially modulating neuroendocrine and behavioral processes relevant to aging. Future mechanistic and longitudinal studies are still needed to determine whether modulation of PYY signaling can mitigate frailty risk. Several novel biological pathways identified included the collagen-containing extracellular matrix (pivotal for maintaining tissue structural integrity and stability)[26,27] and the vesicle lumen (crucial for cellular transport and signaling).[28,29] Together, these findings advance understanding of frailty biology and highlight promising targets for further mechanistic and therapeutic exploration.

Please cite this article in press as: Jia et al., Plasma proteomic signature of frailty in 50,506 adults, Cell Metabolism (2026), https://doi.org/10.1016/j.cmet.2026.02.013

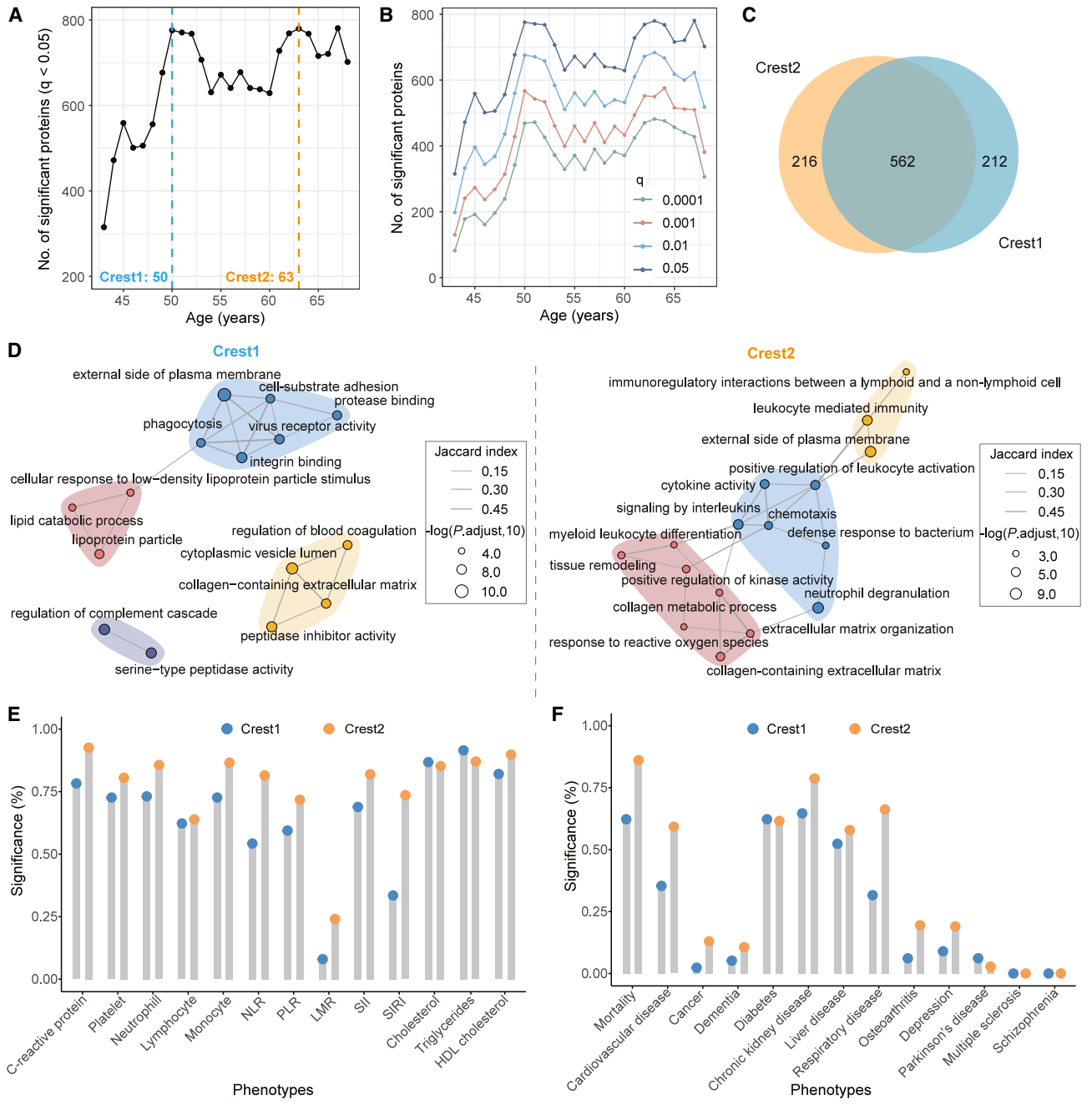

Figure 7. Biphasic waves of frailty-associated proteomic changes during aging

(A) Age-dependent changes of frailty-associated proteins, showing two distinct peaks at 50 and 63 years. The *y* axis displays the count of differentially expressed proteins.

(B) Robustness analysis demonstrating consistent detection of proteomic waves across multiple significance thresholds ($q < 0.0001$, 0.001, 0.01, and 0.05).

(C) Venn diagram quantifying overlap between proteins identified in the 50- and 63-year peaks.

(D) Pathway enrichment and module analysis for proteins specific to each crest.

(E and F) Bar plots showing the proportions of significant associations between crest-specific proteins and metabolic, inflammatory indicators (E) and age-related diseases (F), assessed by linear regression and Cox proportional hazards models, respectively.

Our newly developed PFS demonstrated predictive ability for multiple incident diseases comparable to or even exceeding conventional risk factors, while also providing additional predictive value beyond these established factors. These findings underscore the potential of PFS, particularly the parsimonious PFS93 model, serving both as a streamlined alternative for conventional risk assessments and as a complementary tool to enhance multi-disease risk stratification. Notably, PFS

Please cite this article in press as: Jia et al., Plasma proteomic signature of frailty in 50,506 adults, Cell Metabolism (2026), https://doi.org/10.1016/j.cmet.2026.02.013

outperformed traditional FI for most disease categories, particularly circulatory diseases and endocrine, nutritional, and metabolic disorders, highlighting the inherent advantage of proteomics in capturing dynamic molecular changes[30] and the broader applicability of PFS as a robust tool for frailty assessment. By contrast, the traditional FI, which incorporates clinical and functional measures,[4] better captured chronic physical and psychological impairments associated with musculoskeletal and mental health conditions.

Our study advances the risk profiles of frailty by systematically evaluating 99 potentially modifiable factors across six categories.[2,31] The broad responsiveness of PFS to these factors underscores its potential as a versatile biomarker of aging,[32,33] highlighting the importance of multidimensional interventions for frailty mitigation. Interestingly, PFS and traditional FI exhibited distinct exposome association patterns. PFS demonstrates particular sensitivity to factors (e.g., lifestyle and physical measures) that typically require extended periods to manifest phenotypically, suggesting its ability to identify molecular perturbations preceding clinical manifestations.[34] This preclinical sensitivity enables more timely evaluation of intervention efficacy and optimization of therapeutic strategies, representing a significant advantage over traditional FI's phenotype-dependent assessments that are subject to reporting biases and delayed manifestations. Conversely, the traditional FI demonstrates the significance of monitoring interventions targeting mental health and sleep quality, such as cognitive behavioral therapy and social support programs. Together with the aforementioned findings on disease prediction, these divergent exposome patterns suggest the complementary potential of PFS and FI for holistic frailty assessment, disease prediction, and the evaluation of intervention effectiveness, ultimately enabling more personalized frailty prevention and management strategies.

Frailty represents a multisystem manifestation of accelerated aging, making it inherently difficult to disentangle from aging and overall health deterioration.[1] Nevertheless, when compared with published proteomic aging studies, the PFS captures both overlapping and unique biological information, as evidenced by its moderate correlations with established proteomic aging clocks and additional predictive value for multiple diseases. Notably, PFS demonstrates superior predictive performance for most diseases compared with so-called first-generation clocks trained to predict age, while achieving comparable or even greater accuracy relative to second-generation clocks designed to predict mortality. Together, these findings suggest that PFS is not merely a proxy for general aging but instead captures a partially distinct proteomic signature reflecting the multisystem functional vulnerability that characterizes frailty.

Our longitudinal analysis reveals distinct progression patterns between PFS and traditional FI. The PFS exhibits an age- and baseline frailty severity-dependent acceleration in progression rate, aligning with the cumulative damage theory of aging, where molecular dysregulation establishes a self-reinforcing feedback loop that exacerbates age-related diseases.[35] By contrast, FI maintains a relatively constant progression rate irrespective of age or baseline frailty—consistent with prior studies.[36,37] This divergence underscores fundamental differences in what these indices measure. By capturing dynamic molecular responses to age-related stressors,[38] PFS identifies early, preclinical frailty manifestations that precede overt functional decline. By contrast, FI relies on clinical deficits and thus is less sensitive when functional impairment remains subclinical. Additionally, its progression rate may be constrained by ceiling effects in advanced frailty cases.[39] This dissociation implies that molecular frailty manifests earlier than clinical frailty and is less affected by ceiling effects, but further research is required to fully understand the predictive value of molecular frailty progression and its underlying mechanisms.

Our study identifies two critical biological windows for frailty intervention. Unlike previous reports of proteomic change crests at 30–40 years in general aging (e.g., Lehallier et al. reported crests at 34, 60, and 78 years[40]), we found frailty-associated proteomic changes peak later—first in the late fourth decade (~50 years) and then consistently at ~60 years. This delayed onset (peaking at 50 vs. 30–40 years) may be attributed to the healthier baseline status of the UKB participants.[41] Moreover, this discrepancy suggests that frailty may represent a distinct physiological process with its own temporal trajectory, rather than simply reflecting accelerated aging. Frailty preventive strategies may need different timing than general anti-aging interventions. Notably, the proteins of these two peaks exhibited stage-specific pathway enrichments, i.e., metabolic and signaling pathways vs. immune-related pathways. This finding suggests that midlife may represent a critical phase for developing metabolic dysregulation that predisposes to later frailty, whereas later life exhibits a transition from metabolic to inflammatory frailty mechanisms.[40] The identification of these two critical windows enables early, pathway-specific interventions targeting distinct biological phases of frailty prior to clinical onset. Note, however, that these conclusions are based on cross-sectional data and should be interpreted cautiously, requiring further longitudinal validation.

Limitations of the study

Some limitations in this study should be noted. First, while we characterized plasma proteomic signatures of frailty, its association with tissue-specific protein expression remains uncertain given known inter-tissue variability.[42] Although we employed an established pathway analysis method to eliminate redundant pathways and identified novel functional modules, the plasma-based assay inherently over-represents secreted proteins (particularly immune-related molecules) while under-representing other biological processes, potentially obscuring some molecular mechanisms. Second, external validation of PFS is lacking due to limited availability of large-scale cohorts with comprehensive frailty assessments and Olink large panel proteomic data. Nevertheless, the robustness of our findings is supported by the use of a 10-fold iterative scheme, cross-validation, and sensitivity analyses. Third, while we accounted for numerous modifiable risk factors, certain factors may have been unintentionally neglected. Residual confounding may persist due to collinearities among these factors. Meanwhile, the cross-sectional design precludes causal inference. Finally, the majority of participants in the UKB were White British and tended to be healthier and wealthier.[41] Further proteomic studies in large-scale non-European ancestral cohorts are needed.

In summary, this study delineates the most comprehensive plasma proteomic landscape of frailty in the largest sample to date, bridging key knowledge gaps in understanding the molecular mechanisms of frailty and offering translational potential for developing robust biomarkers and personalized therapeutic strategies to promote healthy aging. More importantly, we introduce PFS, a novel proteomic-based frailty measure with superior predictive capacity for incident diseases, broad responsiveness to diverse modifiable risk factors, and high sensitivity to preclinical molecular dynamics across aging. As a plasma-based assay derived from routine blood sampling, PFS exhibits the advantages of objective quantification and high accessibility. Although current proteomic profiling requires specialized platforms, these technologies are increasingly accessible in research and emerging clinical settings. With continued advancements in scalability and cost-efficiency, PFS, particularly the parsimonious PFS93, holds promise for integration into future clinical workflows and for advancing precision medicine in aging and frailty research.

RESOURCE AVAILABILITY

Lead contact

Requests for further information and resources should be directed to and will be fulfilled by the lead contact, Zuyun Liu (zuyunliu@zju.edu.cn).

Materials availability

This study did not generate any new, unique reagents.

Data and code availability

- Data from UKB are available upon application at https://www.ukbiobank.ac.uk/use-our-data/apply-for-access/. The main data used in this study were accessed under application number 61856. Data from the Swedish Twin Registry, an international research resource, are available upon application at https://ki.se/en/research/swedish-twin-registry-for-researchers. The pQTL data were obtained from the UKB-PPP.[15] The GWAS summary statistics for frailty are publicly accessible at https://doi.org/10.6084/m9.figshare.9204998.
- Source data underlying graphs related to Figures 2, 3, 4, 5, 6, 7, S2–S4, and S6–S8 are available as Data S1.
- All key original code has been deposited at GitHub and is publicly available at https://github.com/XueqingJia/Proteomics_frailty as of the date of publication.
- Any additional information required to reanalyze the data reported in this paper is available from the lead contact upon request.

ACKNOWLEDGMENTS

This research is supported by grants from the National Natural Science Foundation of China (72374180 and 82401856); the "Pioneer" and "Leading Goose" R&D Programs of Zhejiang Province (2026C02A1147 and 2025C02104); the Hangzhou Meilian Medical Co., Ltd.; the Shanghai Municipal Science and Technology Major Project (2017SHZDZX01); and the Zhejiang Provincial Applied Basic Research Program-"Xinmiao" Project. The Swedish Twin Registry is managed by Karolinska Institutet and receives funding through the Swedish Research Council under the grant no. 2021-00180. S.H. is supported by the Swedish Research Council (2022-01608) and the Karolinska Institutet. H.H. is supported by the SciLifeLab & Wallenberg Data Driven Life Science Program (grant KAW2024.0159). We acknowledge the Swedish Twin Registry for access to data. We are particularly indebted to the Computing for the Future at Fudan (CFFF) platform for their critical support in data management and computational processing.

AUTHOR CONTRIBUTIONS

Z.L. designed and supervised the study. X.J., W.G., H.H., and J.Z. analyzed the data. X.J. and Y.Z. drafted the manuscript. X.J., W.G., H.H., Z.H., S.H., and Z.L. interpreted the results. All authors revised the manuscript. Z.L. took responsibility for the content of the article. All authors have read and approved the submitted version of the manuscript.

DECLARATION OF INTERESTS

The authors declare no competing interests.

STAR★METHODS

Detailed methods are provided in the online version of this paper and include the following:

- KEY RESOURCES TABLE
- EXPERIMENTAL MODEL AND STUDY PARTICIPANT DETAILS
  - Study participants
- METHOD DETAILS
  - Plasma proteomic measurements
  - Frailty assessment
  - Ascertainment of health-related outcomes
  - Modifiable factors
  - Age-related chronic diseases, metabolic indicators, and inflammatory markers
  - Covariates
- QUANTIFICATION AND STATISTICAL ANALYSIS
  - Participants characteristics
  - PWAS of frailty
  - Pathway enrichment analysis and functional module identification
  - The development of PFS model
  - Iterative feature evaluation and recursive elimination
  - The predictive performance of the PFS and FI for health-related outcomes
  - Associations of modifiable factors with PFS and FI
  - Comparisons with existing proteomic aging studies
  - Calculation of PFS (and FI) change rate with revisit proteome data
  - DE–SWAN
  - Organ-specific proteins enrichment analyses
  - Proteome-wide MR analyses
  - Colocalization analyses
  - SMR analysis

SUPPLEMENTAL INFORMATION

Supplemental information can be found online at https://doi.org/10.1016/j.cmet.2026.02.013.

Received: June 18, 2025
Revised: November 21, 2025
Accepted: February 17, 2026

REFERENCES

1. Kim, D.H., and Rockwood, K. (2024). Frailty in older adults. N. Engl. J. Med. *391*, 538–548. https://doi.org/10.1056/NEJMra2301292.
2. Hoogendijk, E.O., Afilalo, J., Ensrud, K.E., Kowal, P., Onder, G., and Fried, L.P. (2019). Frailty: implications for clinical practice and public health. Lancet *394*, 1365–1375. https://doi.org/10.1016/S0140-6736(19)31786-6.
3. Fried, L.P., Tangen, C.M., Walston, J., Newman, A.B., Hirsch, C., Gottdiener, J., Seeman, T., Tracy, R., Kop, W.J., Burke, G., et al. (2001). Frailty in older adults: evidence for a phenotype. J. Gerontol. A Biol. Sci. Med. Sci. *56*, M146–M156. https://doi.org/10.1093/gerona/56.3.m146.

4. Mitnitski, A.B., Mogilner, A.J., and Rockwood, K. (2001). Accumulation of deficits as a proxy measure of aging. ScientificWorldJournal *1*, 323–336. https://doi.org/10.1100/tsw.2001.58.

5. Mak, J.K.L., Kananen, L., Qin, C., Kuja-Halkola, R., Tang, B., Lin, J., Wang, Y., Jääskeläinen, T., Koskinen, S., Lu, Y., et al. (2023). Unraveling the metabolic underpinnings of frailty using multicohort observational and Mendelian randomization analyses. Aging Cell *22*, e13868. https://doi.org/10.1111/acel.13868.

6. Bålsrud, P., Ulven, S.M., Ottestad, I., Retterstøl, K., Schwab, U., and Holven, K.B. (2024). Association between inflammatory markers, body composition and frailty in home-dwelling elderly: an 8-year follow-up study. GeroScience *46*, 5629–5641. https://doi.org/10.1007/s11357-024-01279-w.

7. El Assar, M., Rodríguez-Sánchez, I., Álvarez-Bustos, A., and Rodríguez-Mañas, L. (2024). Biomarkers of frailty. Mol. Aspects Med. *97*, 101271. https://doi.org/10.1016/j.mam.2024.101271.

8. Santos, R., Ursu, O., Gaulton, A., Bento, A.P., Donadi, R.S., Bologa, C.G., Karlsson, A., Al-Lazikani, B., Hersey, A., Oprea, T.I., et al. (2017). A comprehensive map of molecular drug targets. Nat. Rev. Drug Discov. *16*, 19–34. https://doi.org/10.1038/nrd.2016.230.

9. Deng, Y.-T., You, J., He, Y., Zhang, Y., Li, H.-Y., Wu, X.-R., Cheng, J.-Y., Guo, Y., Long, Z.-W., Chen, Y.-L., et al. (2025). Atlas of the plasma proteome in health and disease in 53,026 adults. Cell *188*, 253–271.e7. https://doi.org/10.1016/j.cell.2024.10.045.

10. Perry, A.S., Zhao, S., Gajjar, P., Murthy, V.L., Lehallier, B., Miller, P., Nair, S., Neill, C., Carr, J.J., Fearon, W., et al. (2023). Proteomic architecture of frailty across the spectrum of cardiovascular disease. Aging Cell *22*, e13978. https://doi.org/10.1111/acel.13978.

11. Sathyan, S., Ayers, E., Gao, T., Milman, S., Barzilai, N., and Verghese, J. (2020). Plasma proteomic profile of frailty. Aging Cell *19*, e13193. https://doi.org/10.1111/acel.13193.

12. Liu, F., Austin, T.R., Schrack, J.A., Chen, J., Walston, J., Mathias, R.A., Grams, M., Odden, M.C., Newman, A., Psaty, B.M., et al. (2023). Late-life plasma proteins associated with prevalent and incident frailty: A proteomic analysis. Aging Cell *22*, e13975. https://doi.org/10.1111/acel.13975.

13. Xu, J., Liu, J., Tang, J., Liao, J., Liu, X., Odden, M.C., and Wu, C. (2025). Plasma proteomic signature of risk and prognosis of frailty in the UK Biobank. GeroScience *47*, 2365–2381. https://doi.org/10.1007/s11357-024-01415-6.

14. Hoover, M., Rotermann, M., Sanmartin, C., and Bernier, J. (2013). Validation of an index to estimate the prevalence of frailty among community-dwelling seniors. Health Rep. *24*, 10–17.

15. Sun, B.B., Chiou, J., Traylor, M., Benner, C., Hsu, Y.-H., Richardson, T.G., Surendran, P., Mahajan, A., Robins, C., Vasquez-Grinnell, S.G., et al. (2023). Plasma proteomic associations with genetics and health in the UK Biobank. Nature *622*, 329–338. https://doi.org/10.1038/s41586-023-06592-6.

16. Ferrucci, L., and Fabbri, E. (2018). Inflammageing: chronic inflammation in ageing, cardiovascular disease, and frailty. Nat. Rev. Cardiol. *15*, 505–522. https://doi.org/10.1038/s41569-018-0064-2.

17. Shen, X., Wang, C., Zhou, X., Zhou, W., Hornburg, D., Wu, S., and Snyder, M.P. (2024). Nonlinear dynamics of multi-omics profiles during human aging. Nat Aging *4*, 1619–1634. https://doi.org/10.1038/s43587-024-00692-2.

18. Oh, H.S.-H., Rutledge, J., Nachun, D., Pálovics, R., Abiose, O., Moran-Losada, P., Channappa, D., Urey, D.Y., Kim, K., Sung, Y.J., et al. (2023). Organ aging signatures in the plasma proteome track health and disease. Nature *624*, 164–172. https://doi.org/10.1038/s41586-023-06802-1.

19. Atkins, J.L., Jylhävä, J., Pedersen, N.L., Magnusson, P.K., Lu, Y., Wang, Y., Hägg, S., Melzer, D., Williams, D.M., and Pilling, L.C. (2021). A genome-wide association study of the frailty index highlights brain pathways in ageing. Aging Cell *20*, e13459. https://doi.org/10.1111/acel.13459.

20. Oh, H.S.-H., Le Guen, Y., Rappoport, N., Urey, D.Y., Farinas, A., Rutledge, J., Channappa, D., Wagner, A.D., Mormino, E., Brunet, A., et al. (2025). Plasma proteomics links brain and immune system aging with healthspan and longevity. Nat. Med. *31*, 2703–2711. https://doi.org/10.1038/s41591-025-03798-1.

21. Goeminne, L.J.E., Vladimirova, A., Eames, A., Tyshkovskiy, A., Argentieri, M.A., Ying, K., Moqri, M., and Gladyshev, V.N. (2025). Plasma protein-based organ-specific aging and mortality models unveil diseases as accelerated aging of organismal systems. Cell Metab. *37*, 205–222.e6. https://doi.org/10.1016/j.cmet.2024.10.005.

22. Gheller, B.J., Blum, J.E., Merritt, E.K., Cummings, B.P., and Thalacker-Mercer, A.E. (2019). Peptide YY (PYY) is expressed in human skeletal muscle tissue and expanding human muscle progenitor cells. Front. Physiol. *10*, 188. https://doi.org/10.3389/fphys.2019.00188.

23. Liu, W.W., Reicher, N., Alway, E., Rupprecht, L.E., Weng, P., Schaefgen, C., Klein, M.E., Villalobos, J.A., Puerto-Hernandez, C., Kiesling Altún, Y.G., et al. (2025). A gut sense for a microbial pattern regulates feeding. Nature *645*, 729–736. https://doi.org/10.1038/s41586-025-09301-7.

24. Le Roux, C.W., and Bloom, S.R. (2005). Peptide YY, appetite and food intake. Proc. Nutr. Soc. *64*, 213–216. https://doi.org/10.1079/pns2005427.

25. Manning, S., and Batterham, R.L. (2014). The role of gut hormone peptide YY in energy and glucose homeostasis: twelve years on. Annu. Rev. Physiol. *76*, 585–608. https://doi.org/10.1146/annurev-physiol-021113-170404.

26. Yang, C., Hillas, P.J., Báez, J.A., Nokelainen, M., Balan, J., Tang, J., Spiro, R., and Polarek, J.W. (2004). The application of recombinant human collagen in tissue engineering. BioDrugs *18*, 103–119. https://doi.org/10.2165/00063030-200418020-00004.

27. Gelse, K., Pöschl, E., and Aigner, T. (2003). Collagens–structure, function, and biosynthesis. Adv. Drug Deliv. Rev. *55*, 1531–1546. https://doi.org/10.1016/j.addr.2003.08.002.

28. Hou, J., Chen, K.-X., He, C., Li, X.-X., Huang, M., Jiang, Y.-Z., Jiao, Y.-R., Xiao, Q.-N., He, W.-Z., Liu, L., et al. (2024). Aged bone marrow macrophages drive systemic aging and age-related dysfunction via extracellular vesicle-mediated induction of paracrine senescence. Nat Aging *4*, 1562–1581. https://doi.org/10.1038/s43587-024-00694-0.

29. Yin, Y., Chen, H., Wang, Y., Zhang, L., and Wang, X. (2021). Roles of extracellular vesicles in the aging microenvironment and age-related diseases. J. Extracell. Vesicles *10*, e12154. https://doi.org/10.1002/jev2.12154.

30. Walker, K.A., Chen, J., Zhang, J., Fornage, M., Yang, Y., Zhou, L., Grams, M.E., Tin, A., Daya, N., Hoogeveen, R.C., et al. (2021). Large-scale plasma proteomic analysis identifies proteins and pathways associated with dementia risk. Nat Aging *1*, 473–489. https://doi.org/10.1038/s43587-021-00064-0.

31. Feng, Z., Lugtenberg, M., Franse, C., Fang, X., Hu, S., Jin, C., and Raat, H. (2017). Risk factors and protective factors associated with incident or increase of frailty among community-dwelling older adults: A systematic review of longitudinal studies. PLoS One *12*, e0178383. https://doi.org/10.1371/journal.pone.0178383.

32. Moqri, M., Herzog, C., Poganik, J.R., Ying, K., Justice, J.N., Belsky, D.W., Higgins-Chen, A.T., Chen, B.H., Cohen, A.A., Fuellen, G., et al. (2024). Validation of biomarkers of aging. Nat. Med. *30*, 360–372. https://doi.org/10.1038/s41591-023-02784-9.

33. Moqri, M., Herzog, C., Poganik, J.R., Biomarkers; Aging Consortium, Justice, J., Belsky, D.W., Higgins-Chen, A., Moskalev, A., Fuellen, G., Cohen, A.A., et al. (2023). Biomarkers of aging for the identification and evaluation of longevity interventions. Cell *186*, 3758–3775. https://doi.org/10.1016/j.cell.2023.08.003.

34. Carrasco-Zanini, J., Pietzner, M., Davitte, J., Surendran, P., Croteau-Chonka, D.C., Robins, C., Torralbo, A., Tomlinson, C., Grünschläger, F., Fitzpatrick, N., et al. (2024). Proteomic signatures improve risk prediction for common and rare diseases. Nat. Med. *30*, 2489–2498. https://doi.org/10.1038/s41591-024-03142-z.

35. Belikov, A.V. (2019). Age-related diseases as vicious cycles. Ageing Res. Rev. *49*, 11–26. https://doi.org/10.1016/j.arr.2018.11.002.

36. Hoogendijk, E.O., Rockwood, K., Theou, O., Armstrong, J.J., Onwuteaka-Philipsen, B.D., Deeg, D.J.H., and Huisman, M. (2018). Tracking changes in frailty throughout later life: results from a 17-year longitudinal study in the Netherlands. Age Ageing *47*, 727–733. https://doi.org/10.1093/ageing/afy081.

37. Mitnitski, A., and Rockwood, K. (2016). The rate of aging: the rate of deficit accumulation does not change over the adult life span. Biogerontology *17*, 199–204. https://doi.org/10.1007/s10522-015-9583-y.

38. Kemoun, P., Ader, I., Planat-Benard, V., Dray, C., Fazilleau, N., Monsarrat, P., Cousin, B., Paupert, J., Ousset, M., Lorsignol, A., et al. (2022). A gero-physiology perspective on healthy ageing. Ageing Res. Rev. *73*, 101537. https://doi.org/10.1016/j.arr.2021.101537.

39. Howlett, S.E., Rutenberg, A.D., and Rockwood, K. (2021). The degree of frailty as a translational measure of health in aging. Nat. Aging *1*, 651–665. https://doi.org/10.1038/s43587-021-00099-3.

40. Lehallier, B., Gate, D., Schaum, N., Nanasi, T., Lee, S.E., Yousef, H., Moran Losada, P., Berdnik, D., Keller, A., Verghese, J., et al. (2019). Undulating changes in human plasma proteome profiles across the lifespan. Nat. Med. *25*, 1843–1850. https://doi.org/10.1038/s41591-019-0673-2.

41. Fry, A., Littlejohns, T.J., Sudlow, C., Doherty, N., Adamska, L., Sprosen, T., Collins, R., and Allen, N.E. (2017). Comparison of sociodemographic and health-related characteristics of UK Biobank participants with those of the general population. Am. J. Epidemiol. *186*, 1026–1034. https://doi.org/10.1093/aje/kwx246.

42. Uhlén, M., Fagerberg, L., Hallström, B.M., Lindskog, C., Oksvold, P., Mardinoglu, A., Sivertsson, Å., Kampf, C., Sjöstedt, E., Asplund, A., et al. (2015). Proteomics. Tissue-based map of the human proteome. Science *347*, 1260419. https://doi.org/10.1126/science.1260419.

43. Sudlow, C., Gallacher, J., Allen, N., Beral, V., Burton, P., Danesh, J., Downey, P., Elliott, P., Green, J., Landray, M., et al. (2015). UK biobank: an open access resource for identifying the causes of a wide range of complex diseases of middle and old age. PLoS Med. *12*, e1001779. https://doi.org/10.1371/journal.pmed.1001779.

44. Magnusson, P.K.E., Almqvist, C., Rahman, I., Ganna, A., Viktorin, A., Walum, H., Halldner, L., Lundström, S., Ullén, F., Långström, N., et al. (2013). The Swedish Twin Registry: establishment of a biobank and other recent developments. Twin Res. Hum. Genet. *16*, 317–329. https://doi.org/10.1017/thg.2012.104.

45. Zhu, Z., Zhang, F., Hu, H., Bakshi, A., Robinson, M.R., Powell, J.E., Montgomery, G.W., Goddard, M.E., Wray, N.R., Visscher, P.M., et al. (2016). Integration of summary data from GWAS and eQTL studies predicts complex trait gene targets. Nat. Genet. *48*, 481–487. https://doi.org/10.1038/ng.3538.

46. Hastie, T., Tibshirani, R., Narasimhan, B., and Chu, G. (2023). impute: Imputation for microarray data. R package version 1.76.0. https://bioconductor.org/packages/impute.

47. Yu, G., Wang, L.-G., Han, Y., and He, Q.-Y. (2012). clusterProfiler: an R package for comparing biological themes among gene clusters. OMICS *16*, 284–287. https://doi.org/10.1089/omi.2011.0118.

48. Gu, Z., and Hübschmann, D. (2023). simplifyEnrichment: a Bioconductor package for clustering and visualizing functional enrichment results. Genomics Proteomics Bioinformatics *21*, 190–202. https://doi.org/10.1016/j.gpb.2022.04.008.

49. Csárdi G., Nepusz T., Traag V., Horvát S., Zanini F., Noom D., Müller K., Schoch D., Salmon M. (2026). igraph: Network Analysis and Visualization in R, R package version 2.0.3, https://CRAN.R-project.org/package=igraph

50. Kuhn, M. (2008). Building predictive models in R using the caret package. J. Stat. Soft. *28*, 1–26. https://doi.org/10.18637/jss.v028.i05.

51. Meyer, D., and Buchta, C. (2022). proxy: Distance and Similarity Measures. R package version 0.4-27. https://CRAN.R-project.org/package=proxy.

52. Therneau, T. (2024). A package for survival analysis in R. R package version 3.6-4. https://cran.r-project.org/package=survival.

53. Kang, L., Chen, W., Petrick, N.A., and Gallas, B.D. (2015). Comparing two correlated C indices with right-censored survival outcome: a one-shot nonparametric approach. Stat. Med. *34*, 685–703. https://doi.org/10.1002/sim.6370.

54. Bates, D., Mächler, M., Bolker, B., and Walker, S. (2015). Fitting linear mixed-effects models using lme4. J. Stat. Soft. *67*, 1–48. https://doi.org/10.18637/jss.v067.i01.

55. Hemani, G., Zheng, J., Elsworth, B., Wade, K.H., Baird, D., Haberland, V., Laurin, C., Burgess, S., Bowden, J., Langdon, R., et al. (2018). The MR-Base platform supports systematic causal inference across the human phenome. eLife *7*, e34408. https://doi.org/10.7554/eLife.34408.

56. Wallace, C. (2021). A more accurate method for colocalisation analysis allowing for multiple causal variants. PLoS Genet. *17*, e1009440. https://doi.org/10.1371/journal.pgen.1009440.

57. Elliott, P., and Peakman, T.C.; UK Biobank (2008). The UK Biobank sample handling and storage protocol for the collection, processing and archiving of human blood and urine. Int. J. Epidemiol. *37*, 234–244. https://doi.org/10.1093/ije/dym276.

58. Wik, L., Nordberg, N., Broberg, J., Björkesten, J., Assarsson, E., Henriksson, S., Grundberg, I., Pettersson, E., Westerberg, C., Liljeroth, E., et al. (2021). Proximity extension assay in combination with next-generation sequencing for high-throughput proteome-wide analysis. Mol. Cell. Proteomics *20*, 100168. https://doi.org/10.1016/j.mcpro.2021.100168.

59. Messner, C.B., Demichev, V., Bloomfield, N., Yu, J.S.L., White, M., Kreidl, M., Egger, A.-S., Freiwald, A., Ivosev, G., Wasim, F., et al. (2021). Ultra-fast proteomics with scanning SWATH. Nat. Biotechnol. *39*, 846–854. https://doi.org/10.1038/s41587-021-00860-4.

60. Williams, D.M., Jylhävä, J., Pedersen, N.L., and Hägg, S. (2019). A frailty index for UK Biobank participants. J. Gerontol. A Biol. Sci. Med. Sci. *74*, 582–587. https://doi.org/10.1093/gerona/gly094.

61. Searle, S.D., Mitnitski, A., Gahbauer, E.A., Gill, T.M., and Rockwood, K. (2008). A standard procedure for creating a frailty index. BMC Geriatr. *8*, 24. https://doi.org/10.1186/1471-2318-8-24.

62. Li, X., Ploner, A., Karlsson, I.K., Liu, X., Magnusson, P.K.E., Pedersen, N.L., Hägg, S., and Jylhävä, J. (2019). The frailty index is a predictor of cause-specific mortality independent of familial effects from midlife onwards: a large cohort study. BMC Med. *17*, 94. https://doi.org/10.1186/s12916-019-1331-8.

63. Han, H., Cao, Y., Feng, C., Zheng, Y., Dhana, K., Zhu, S., Shang, C., Yuan, C., and Zong, G. (2022). Association of a healthy lifestyle with all-cause and cause-specific mortality among individuals with type 2 diabetes: a prospective study in UK Biobank. Diabetes Care *45*, 319–329. https://doi.org/10.2337/dc21-1512.

64. Jia, X., Fan, J., Wu, X., Cao, X., Ma, L., Abdelrahman, Z., Zhao, F., Zhu, H., Bizzarri, D., van den Akker, E.B.V.D., et al. (2024). A novel metabolomic aging clock predicting health outcomes and its genetic and modifiable factors. Adv. Sci. (Weinh) *11*, e2406670. https://doi.org/10.1002/advs.202406670.

65. Tian, Y.E., Cropley, V., Maier, A.B., Lautenschlager, N.T., Breakspear, M., and Zalesky, A. (2023). Heterogeneous aging across multiple organ systems and prediction of chronic disease and mortality. Nat. Med. *29*, 1221–1231. https://doi.org/10.1038/s41591-023-02296-6.

66. Wu, T., Hu, E., Xu, S., Chen, M., Guo, P., Dai, Z., Feng, T., Zhou, L., Tang, W., Zhan, L., et al. (2021). clusterProfiler 4.0: A universal enrichment tool for interpreting omics data. Innovation (Camb.) *2*, 100141. https://doi.org/10.1016/j.xinn.2021.100141.

67. Duggan, M.R., Peng, Z., Sipilä, P.N., Lindbohm, J.V., Chen, J., Lu, Y., Davatzikos, C., Erus, G., Hohman, T.J., Andrews, S.J., et al. (2024). Proteomics identifies potential immunological drivers of postinfection brain atrophy and cognitive decline. Nat Aging *4*, 1263–1278. https://doi.org/10.1038/s43587-024-00682-4.

68. Watanabe, K., Wilmanski, T., Diener, C., Earls, J.C., Zimmer, A., Lincoln, B., Hadlock, J.J., Lovejoy, J.C., Gibbons, S.M., Magis, A.T., et al. (2023). Multiomic signatures of body mass index identify heterogeneous health phenotypes and responses to a lifestyle intervention. Nat. Med. *29*, 996–1008. https://doi.org/10.1038/s41591-023-02248-0.

69. Johnson, A.A., Shokhirev, M.N., Wyss-Coray, T., and Lehallier, B. (2020). Systematic review and analysis of human proteomics aging studies unveils a novel proteomic aging clock and identifies key processes that change with age. Ageing Res. Rev. *60*, 101070. https://doi.org/10.1016/j.arr.2020.101070.

70. Coenen, L., Lehallier, B., de Vries, H.E., and Middeldorp, J. (2023). Markers of aging: Unsupervised integrated analyses of the human plasma proteome. Front. Aging *4*, 1112109. https://doi.org/10.3389/fragi.2023.1112109.

71. Argentieri, M.A., Xiao, S., Bennett, D., Winchester, L., Nevado-Holgado, A.J., Ghose, U., Albukhari, A., Yao, P., Mazidi, M., Lv, J., et al. (2024). Proteomic aging clock predicts mortality and risk of common age-related diseases in diverse populations. Nat. Med. *30*, 2450–2460. https://doi.org/10.1038/s41591-024-03164-7.

72. Zhu, Z., Zhu, X., Liu, C.-L., Shi, H., Shen, S., Yang, Y., Hasegawa, K., Camargo, C.A., and Liang, L. (2019). Shared genetics of asthma and mental health disorders: a large-scale genome-wide cross-trait analysis. Eur. Respir. J. *54*, 1901507. https://doi.org/10.1183/13993003.01507-2019.

73. Wu, Y., Zeng, J., Zhang, F., Zhu, Z., Qi, T., Zheng, Z., Lloyd-Jones, L.R., Marioni, R.E., Martin, N.G., Montgomery, G.W., et al. (2018). Integrative analysis of omics summary data reveals putative mechanisms underlying complex traits. Nat. Commun. *9*, 918. https://doi.org/10.1038/s41467-018-03371-0.

Please cite this article in press as: Jia et al., Plasma proteomic signature of frailty in 50,506 adults, Cell Metabolism (2026), https://doi.org/10.1016/j.cmet.2026.02.013

STAR★METHODS

KEY RESOURCES TABLE

REAGENT or RESOURCE	SOURCE	IDENTIFIER
Deposited data		
UK Biobank data	Sudlow et al.[43]	https://www.ukbiobank.ac.uk/
GWAS summary statistics for frailty index	Atkins et al.[19]	https://doi.org/10.6084/m9.figshare.9204998
Protein quantitative trait loci (pQTL) data	Sun et al.[15]	https://www.synapse.org/Synapse:syn51364943/wiki/622119
TwinGene data	Magnusson et al.[44]	https://ki.se/en/research/research-infrastructure-and-environments/core-facilities-for-research/the-swedish-twin-registry
Software and algorithms		
Software: R (version 4.3.3)	R Core Team	https://cran.r-project.org/
Software: SMR (version 1.3.1)	Zhu et al.[45]	https://yanglab.westlake.edu.cn/software/smr/
R code	This paper	https://github.com/XueqingJia/Proteomics_frailty
k-nearest neighbor imputation: impute R package (version 1.76.0)	Hastie et al.[46]	https://www.bioconductor.org/packages/release/bioc/html/impute.html
Functional enrichment: clusterProfiler R package (version 4.10.1)	Yu et al.[47]	https://www.bioconductor.org/packages/clusterProfiler
Functional enrichment: simplifyEnrichment R package (version 1.12.0)	Gu et al.[48]	https://github.com/jokergoo/simplifyEnrichment
Network Analysis and Visualization: igraph R package (version 2.0.3)	Csárdi et al.[49]	https://cran.r-project.org/web/packages/igraph/index.html
LASSO: Caret R package version 6.0.94	Kuhn et al.[50]	https://github.com/topepo/caret/
Similarity measures: proxy R package (version 0.4.27)	Meyer et al.[51]	https://cran.r-project.org/web/packages/proxy/index.html
Predictive performance: survival R package (version 3.6.4)	Therneau et al.[52]	https://cran.r-project.org/web/packages/survival/index.html
C-index comparison: compareC R package (version 1.3.2)	Kang et al.[53]	https://cran.r-project.org/web/packages/compareC/index.html
Mixed-effects model: lme4 R package (version 1.1.35.3)	Bates et al.[54]	https://cran.r-project.org/web/packages/lme4/index.html
DEswan analysis: DEswan R package (version 0.0.0.9001)	Lehallier et al.[40]	https://github.com/lehallib/DEswan
Mendelian randomization analyses: TwoSampleMR R package (version 0.6.2)	Hemani et al.[55]	https://github.com/MRCIEU/TwoSampleMR
Colocalization analyses: coloc R package R package (version 5.2.3)	Wallace et al.[56]	https://cran.r-project.org/web/packages/coloc/index.html

EXPERIMENTAL MODEL AND STUDY PARTICIPANT DETAILS

Study participants

The UKB is a prospective, population-based cohort comprising over 500,000 participants aged 40-69 years at baseline, recruited between 2006 and 2010 through 22 assessment centers across the UK. Data were collected via touch-screen questionnaires, physical measurements, biological samples, and linked medical and death register records. Detailed study design and methodology have been reported elsewhere.[43] UKB has approval from the North West Multi-Centre Research Ethics Committee as a Research Tissue Bank approval in 2011 and is renewed every 5 years. All participants have provided signed informed consent.

As an independent external validation cohort, the TwinGene study, a population-based subcohort of the Swedish Twin Registry (STR), recruited Swedish twins born between 1911 and 1958 who had previously participated in the Screening Across the Lifespan

Please cite this article in press as: Jia et al., Plasma proteomic signature of frailty in 50,506 adults, Cell Metabolism (2026), https://doi.org/10.1016/j.cmet.2026.02.013

CellPress
OPEN ACCESS

Twin questionnaire (SALT).[44] Between 2004 and 2008, a total of 12,614 twins were recruited and underwent a basic health checkup, completed a self-reported questionnaire, and provided blood samples. The use of data from the Swedish Twin Registry was approved by the Swedish Ethical Review Authority (Dnr 2022-06634-01).

METHOD DETAILS

Plasma proteomic measurements

The UKB Proteomics Project (UKB-PPP) consortium performed proteomic profiling on blood plasma samples collected from 53,026 participants at baseline, using Olink Explore™ Proximity Extension Assay and next-generation sequencing between April 2021 and February 2022. Stringent quality control (refer to biobank.ndph.ox.ac.uk/ukb/ukb/docs/PPP_Phase_1_QC_dataset_companion_doc.pdf for detailed information) was implemented to enable high-throughput quantification of 2,923 proteins across eight panels: cardiometabolic (I and II), inflammation (I and II), neurology (I and II), and oncology (I and II). The final assay read-out was represented as Normalized Protein eXpression (NPX), which was log-transformed and standardized to ensure comparability across samples and batches and accuracy of measuring low-abundance proteins; higher NPX values indicated higher protein expression. Further detailed protocols for sample handling, assay validation, data processing and quality control procedures were provided in previous publications.[15,57] In this study, we retained 2,911 proteins with $\leq$ 20% missing values. After excluding participants with missing data on > 80% proteins, > 10 frailty items, or covariate information, 50,506 participants were included in the primary analyses. Missing proteomic values were imputed using the k-nearest neighbor algorithm (KNN; k = 10, Euclidean distance) via the *impute.knn* function from the impute R package (v1.76.0). No additional outlier removal was applied beyond the built-in quality control procedures in the UKB Olink proteomics pipeline.

In the TwinGene study, circulating proteins were measured in serum using two different proteomics methods. Olink's oncology I and II panels[58] were utilized for indirect protein level measurement in a subgroup, while SWATH[59] mass spectrometry directly measured protein levels across the complete cohort. In this study, we selected 5,446 participants with available data on 297 proteins overlapping with those significantly associated with FI in the UKB, FI information, along with corresponding FI scores and relevant covariates, for the PWAS replication analyses. We selected 6,211 participants with available data on 351 proteins measured by Olink in both UKB and the TwinGene study, FI information, along with corresponding FI scores, relevant covariates and all-cause mortality data, for the PFS replication analyses.

Frailty assessment

Frailty was assessed using the FI, following the methods proposed by Rockwood et al.[4] In the UKB, the FI was constructed using 49 self-reported items across sensory, cranial, mental well-being, infirmity, cardiometabolic, respiratory, musculoskeletal, immunological, cancer, pain, and gastrointestinal conditions (Table S7).[60] These variables reflect both physiological and mental health, including symptoms, disabilities, and diagnosed diseases. The FI was calculated by dividing the number of deficits present in a participant by the total number of possible deficits, yielding a continuous FI score ranging from 0 to 1. Participants with missing data on more than 10 FI items were excluded. Following validated thresholds,[61] participants were classified as non-frail (FI score < 0.21) and frail (FI score $\geq$ 0.21). In the TwinGene study, the FI was derived from 44 comparable self-reported health items and subsequently calculated using the same method.[62]

Ascertainment of health-related outcomes

Health outcomes were ascertained by linking UKB participants to the National Health Service (NHS) electronic health records using the International Classification of Diseases (ICD)-10 codes. Following the methodology outlined by Deng et al.,[9] we utilized the FinnGen disease endpoints code (https://www.finngen.fi/en/researchers/clinical-endpoints) and adhered to FinnGen's quality control guidelines. This process included pre-defined conditions based on sex and age, as well as exclusions for specific diseases in the control groups. Notably, several diseases originally coded with two decimal places were rounded to one decimal to align with the ICD-10 code format used by UKB. Incident cases were defined as those occurring after baseline assessment, with follow-up time censored at the earliest occurrence of disease diagnosis, death, loss to follow-up, or end of follow-up (October 31, 2022). A total of 655 incident disease endpoints were included in this analysis, with participants diagnosed before baseline being excluded. Detailed quality control criteria and endpoint specifications were shown in Table S5C.

Dates and causes of death in the UKB were ascertained by linking to national death registries. The all-cause and cause-specific mortality (i.e., cancer, CVD, respiratory disease, neurodegenerative disease, digestive disease, and other causes) were classified according to ICD-10 codes (Table S8).[63] Follow-up time was defined as the time from the baseline assessment date to the earliest of the following events: date of death, date of loss to follow-up, or the end of follow-up (December 31, 2022).

Dates of death in the TwinGene study were obtained from the Swedish National Cause of Death Register. Follow-up time was defined as the time from the baseline assessment date to the earliest of the following events: date of death, date of loss to follow-up, or the end of follow-up (February 26, 2024).

Modifiable factors

We considered a total of 99 potentially modifiable factors derived from the UKB baseline survey.[64] Detailed information on the processing of these factors is provided in Table S9. These factors were categorized into six categories: local environment (e.g.,

greenspace percentage, buffer 1000m), psychosocial (e.g., nervous feelings), socioeconomic status (SES) (e.g., TDI), early life and sexual health (e.g., breastfed as a baby), physical measures (e.g., handgrip strength), and lifestyle factors (e.g., healthy diet).

Age-related chronic diseases, metabolic indicators, and inflammatory markers

We tested associations between the proteins of two key crests and health-related traits, including age-related chronic diseases, metabolic indicators, and systemic inflammatory markers. Chronic diseases included CVD, cancer, dementia, diabetes, chronic kidney disease, liver diseases, respiratory disease, osteoarthritis, depression, Parkinson's disease, multiple sclerosis, and schizophrenia. These diseases were selected based on lifelong contribution to substantial health burden or brain-associated illness burden (i.e., depression and schizophrenia) in older adults.[65] Metabolic indicators included TC, TG, and high-density lipoprotein cholesterol. Inflammatory markers included baseline counts of neutrophils, monocytes, platelets, and lymphocytes, and level of C-reactive protein. We further calculated four ratios based on peripheral blood cell counts including NLR (neutrophils/lymphocytes), PLR (platelets/lymphocytes), LMR (lymphocytes/monocytes), SII (neutrophils $\times$ platelets/lymphocytes), and SIRI (neutrophils $\times$ monocytes/lymphocytes).

Covariates

Demographic variables included age, sex (female or male), ethnicity (White or non-White), and educational level (high, intermediate, or low). Lifestyle factors included smoking status (never, previous, or current smoker), alcohol intake frequency (never or special occasions only, 1-3 times monthly, 1-4 times weekly, or daily/almost daily), regular exercise (yes/no), and healthy diet (yes/no). Anthropometric data included body mass index (BMI, kg/m^2), calculated as weight/height.[2] SES was represented by the TDI, assigned based on participants' residential postcodes. The first 20 genetic principal components (PCs) derived from genome-wide genotyping data were included to account for population stratification and genetic background differences.

QUANTIFICATION AND STATISTICAL ANALYSIS

Participants characteristics

We presented the baseline characteristics of the analytic samples overall and by frailty status. Categorical variables are shown as numbers and percentages, and continuous variables are shown as medians with IQRs. Differences between frailty groups were assessed using χ^2 tests for categorical variables and Kruskal-Wallis tests for continuous variables.

PWAS of frailty

Linear regression models were performed to assess the associations between z-scored protein levels (as the predictor) and FI (as the outcome). The β coefficients and corresponding 95% CIs were estimated using two models. Model 1 was adjusted for age, sex, and the first 20 genetic PCs, and Model 2 was additionally adjusted for ethnicity, educational level, TDI, smoking status, alcohol intake frequency, regular exercise, healthy diet, and BMI. The fully adjusted model (Model 2) was used for all primary analyses.

To ensure the robustness of our findings, we conducted several sensitivity analyses: 1) Treating frailty as a dichotomous variable (non-frail vs. frail), with non-frail participants as the reference group; 2) Restricting the analyses to participants with complete data on all FI items; 3) Restricting the analyses to a randomly selected subset to address potential bias from the UKB-PPP sub-cohort composition; 4) Focusing specifically on Caucasians to further mitigate the possibility of population stratification; 5) Incorporating interaction terms (protein $\times$ age or protein $\times$ sex) into the models to examine whether the strength of protein-frailty associations varied by age or sex, beyond their main effects. Additionally, subgroup PWAS analyses were performed separately for males and females, as well as for younger (< 60 years) and older ($\geq$ 60 years) participants, to provide further insights into potential heterogeneity; 6) Repeating the PWAS excluding regular exercise from Model 2, given that difficulty engaging in physical activity may be intrinsic to frailty pathophysiology; and 7) Adding each covariate separately to Model 1 and quantifying the percentage change in protein effect sizes to assess the impact of individual covariates. The attenuation ratio was calculated as:

$$\text{Attenuation ratio} = \frac{\beta_{\text{Model1}} - \beta_{\text{Adjusted}}}{\beta_{\text{Model1}}}$$

where β_{Model1} and β_{Adjusted} are the regression coefficients from Model 1; from Model 1 with the one additional covariate, respectively.

For replication, two linear regression models were used to examine the associations between circulating proteins and the FI in the TwinGene study. Model 1 was adjusted for age and sex, while Model 2 was additionally adjusted for education years, smoking status, and alcohol consumption in the year prior to blood sampling, and BMI. To address the non-independence of observations within twin pairs and account for the twin structure of the data, cluster-robust standard errors were utilized. To better meet the assumptions of linear regression, the FI was log-transformed (with a 0.1 offset) and multiplied by 10 to improve interpretability.

Pathway enrichment analysis and functional module identification

Pathway enrichment analysis was performed using the clusterProfiler R package, referencing the Gene Ontology (GO), Kyoto Encyclopedia of Genes and Genomes (KEGG), and Reactome databases.[66] Adjusted *P values* were calculated using the Benjamini-Hochberg method, with a significance threshold set at < 0.05. To eliminate redundancy, we calculated the similarity between

Please cite this article in press as: Jia et al., Plasma proteomic signature of frailty in 50,506 adults, Cell Metabolism (2026), https://doi.org/10.1016/j.cmet.2026.02.013

enriched GO terms and pathways: the 'Wang' algorithm from the simplifyEnrichment R package was used for GO terms, while the 'jaccard' algorithm was applied to KEGG and Reactome pathways. Community analysis was then conducted using the igraph R package to partition the similarity network into distinct modules based on edge betweenness. Within each module, the pathway or GO term with the smallest adjusted *P value* was selected as the representative one. Then we merged all the remaining pathways from all three databases and repeated the above process by recalculating the similarity using the Jaccard algorithm. Finally, we employed the same approach again to identify overarching functional modules.

The development of PFS model

To develop PFS, we implemented a nested ten-fold iterative LASSO regression scheme using the Caret R package. The outcome was log-transformed (FI + 0.1). Participants were randomly split into ten folds; in each iteration, one fold was designated as the testing (hold-out) set and the remaining nine folds as the training set. Data processing—including imputation and z-score normalization of protein values—along with feature selection and model fitting, was performed exclusively within each training set. This process was iterated across all ten combinations to generate ten fitted sparse models and one hold-out set-derived prediction for each participant. Overfitting was controlled through this nested ten-fold iteration procedure, and hyperparameters were optimized using ten-fold cross-validation within each training set. To ensure balanced splits, we confirmed no significant differences in sociodemographic, lifestyle-related, or genetic background characteristics (i.e., the first 20 genetic PCs) among the ten sets using χ^2 tests for categorical variables and ANOVA for numeric variables (Data S1). Considering that LASSO models can be sensitive to extreme values, we additionally performed a sensitivity analysis in which protein values were Winsorized at the mean ± 5 SD within each training fold prior to model fitting,[67] which yielded virtually identical performance (Figure S8).

Model performance was evaluated using the out-of-sample R^2 and mean absolute error (MAE), calculated from each corresponding hold-out testing set. Pearson's correlation coefficient (r) between the measured and predicted values were computed across all participants. The pairwise Jaccard indices between the protein sets selected across the ten folds were calculated using the *simil* function from the proxy R package.

Iterative feature evaluation and recursive elimination

We performed an iterative LASSO procedure to assess the relative contributions and potential redundancy of individual proteins. At each iteration, the protein retained across all ten folds with the highest absolute mean β-coefficient was removed, and out-of-sample R^2 was recalculated in each fold. This procedure allowed us to assess whether predictive information was broadly distributed across multiple proteins or dominated by a few top predictors.[68]

To derive a parsimonious and interpretable model, we applied RFE based on SHAP values to the 274 proteins consistently selected across all folds. In each iteration, tenfold cross-validated models were trained using the standard scheme described above, and within each fold, the contribution of each protein was quantified as the mean absolute SHAP value across participants. The average R^2 across folds was recorded at each step. The protein with the smallest mean absolute SHAP value was then removed, and the procedure was repeated until only five proteins remained.

The predictive performance of the PFS and FI for health-related outcomes

We then estimated the predictive performance of PFS (including the full PFS and simplified PFS93) and FI for diseases risk. First, PFS and FI were used independently for disease-risk prediction. Performance was quantified by Harrell's C-index using survival R package. Then, four multivariable prediction models with different combinations of PFS and FI and conventional risk factors (age, sex, ethnicity, TDI, smoking status, alcohol intake frequency, BMI, and systolic blood pressure) were built as follows: Model 1 (only conventional risk factors), Model 2 (conventional risk factors + PFS), Model 3 (conventional risk factors + FI) and Model 4 (conventional risk factors + PFS + FI). These models were built using Cox proportional hazards regression for each disease. The differences in Harrell's C-indexes of these models were compared using the compareC R package.

Associations of modifiable factors with PFS and FI

Multivariable linear regression models were used to evaluate the associations between each modifiable factors (independent variable) and PFS or FI (dependent variable). A Bonferroni-corrected significance threshold was applied to identify significant associations ($P < 0.05/99 = 5.05 \times 10^{-4}$). In these analyses, continuous variables were standardized (z-scaled), and results were expressed as β coefficients per 1-SD increase in the corresponding factor. Modifiable factors were further categorized into tertiles, with the lowest tertile serving as the reference group. All models were adjusted for age, sex, and ethnicity. Stratified analyses were performed by age group (< 60 and ≥ 60 years) and sex (male and female).

Comparisons with existing proteomic aging studies

We compared protein composition (restricted to proteins consistently retained across all ten folds in the full PFS and simplified PFS93 model, respectively) and model's predictive performance in our work with those from six large-scale proteomic aging studies. These included three major non-UKB studies: (1) a systematic review that developed a proteomic aging clock using 85 age-associated proteins and validated it in the INTERVAL cohort (Johnson et al.)[69]; (2) a multi-cohort study identifying 273 age-associated proteins across several populations (Coenen et al.)[70]; and (3) a study that developed a 373-protein aging clock using data from the INTERVAL and LonGenity cohorts (Lehallier et al.).[40] We further considered three recently developed proteomic aging clocks based

Please cite this article in press as: Jia et al., Plasma proteomic signature of frailty in 50,506 adults, Cell Metabolism (2026), https://doi.org/10.1016/j.cmet.2026.02.013

on UKB data: (4) a LightGBM-based model comprising 204 proteins trained on age (Argentieri et al.)[71]; (5) a LASSO-based model including 207 proteins trained on age (Oh et al.)[20]; and (6) two elastic net-based models trained separately on age and mortality (Goeminne et al.).[21] For studies providing complete model details (Oh et al.[20] and Goeminne et al.[21]), we reconstructed the published proteomic clocks using the reported coefficients. We then quantified their correlations with PFS using Pearson correlation coefficients, and compared their predictive performance against PFS for the same health-related outcomes examined in the main analyses.

Calculation of PFS (and FI) change rate with revisit proteome data

UKB includes unique follow-up plasma proteomics data for 1,161 participants at their third visits and 1,113 participants at their fourth visits. For longitudinal analyses, we focused on 1,459 proteins with less than 20% missing values across all three visits (first, third, and fourth). We re-trained PFS model using these 1,459 proteins ("feature-reduced" model) in the 50,506 participants at baseline, following the same approach described above.

For analyses of PFS (and FI) change rates, we retained 784 participants with less than 80% missing data in the 1,459 proteins across all three visits and complete visit date information (Field 53). Missing values of proteins were imputed using the KNN method. For each participant at each time point, the PFS prediction was obtained by averaging ten predicted values generated from the baseline LASSO models applied to the processed time-series proteomic data. Change rates of frailty were then calculated based on the following mixed-effects model[21]:

$$\mathrm{FI}\,/\,\mathrm{PFS}_{ij} = \beta^{0} + x_{ij}^{\Delta age}\beta^{slope} + u_{i}^{intercept} + x_{ij}^{\Delta age}u_{i}^{slope} + \varepsilon_{ij}$$

PFS_{ij} (and FI_{ij}) represents the predicted PFS (and FI) for participant i at visit j. The fixed intercept is denoted by β^{0}, and $x_{ij}^{\Delta age}$ represents the difference in age between visit j and the first visit for participant i. The fixed effect β^{slope} captures the average annual change in predicted PFS (and FI). Participant-specific intercepts and slopes are modeled through random effects $u_i^{intercept}$ and u_i^{slope}, respectively, while ε_{ij} represents the random error term. All random effects and error terms are assumed to follow normal distributions. The mixed-effects models were performed using the lmer function from the lme4 R package. For each individual i, the longitudinal slope was calculated as $\widehat{\beta}^{slope} + \widehat{u}_i^{slope}$ (where the hats indicate the estimated values of the corresponding model parameters), corresponding to the average rate of change in PFS (and FI) during the follow-up period.

We then assessed the correlation between the PFS (and FI) change rate and baseline PFS (and FI) using Spearman correlation coefficient. Additionally, we evaluated the association between the PFS (and FI) change rate and accumulated disease counts using linear regression models, adjusting for the covariates listed above. To validate the robustness of our findings, we also calculated the PFS (and FI) change rate by subtracting the previous round from the subsequent round divided by follow-up time.

Next, we defined participants with FI change rates in the highest quintile as accelerated frailty progressors, and those in the remaining quintiles as normal progressors. Using the same threshold derived from the FI change rates, participants were categorized based on their PFS change rates. We classified participants into matched or mismatched groups according to whether their FI- and PFS-based progression status agreed, and then compared the differences in the cumulative number of diseases between the two groups.

DE–SWAN

The DE-SWAN method, implemented using the DEswan R package, was used to quantify nonlinear changes in the frailty-related proteome during aging.[40] Participant ages were rounded, and the analysis was restricted to participants aged 39 to 71 years. A sliding window approach was employed, with a 6-year window comparing molecule levels between groups in parcels of 3 year, then sliding the window in increments of 1 year from young to old age. Differential expression was assessed using the Wilcoxon test, and *P values* were adjusted for multiple comparisons using the Benjamini-Hochberg correction. Covariates including sex, the first 20 genetic PCs, ethnicity, educational level, TDI, smoking status, alcohol intake frequency, regular exercise, healthy diet, and BMI were adjusted in the DE-SWAN analysis. To evaluate the robustness of the results, the algorithm was tested with different q-value thresholds (<0.0001, <0.001, <0.01, and <0.05).

Organ-specific proteins enrichment analyses

Following the methodology by Oh et al.,[18] we mapped the putative organ-specific plasma proteome by defining a protein as organ-specific if its corresponding RNA expression in the Genotype-Tissue Expression (GTEx) database was at least four-fold higher in one organ compared to any others. Fisher's exact test was used to evaluated whether frailty-associated proteins were significantly enriched with specific organs.

Proteome-wide MR analyses

We obtained pQTLs from GWAS summary statistics in the UKB-PPP of 34,557 participants of European ancestry.[15] Cis-pQTLs (variants located within ±1 Mb of the gene encoding the protein) associated with plasma protein levels at genome-wide significance ($P < 5 \times 10^{-8}$) were selected as IVs. To ensure independence, linkage disequilibrium clumping was applied ($r^2 < 0.1$ within the 1 Mb window). We further removed IVs with an *F*-statistic of less than ten to reduce weak instrument bias and removed IVs that were associated with more than five proteins to minimize horizontal pleiotropy. GWAS summary statistics for frailty (measured using FI) were obtained from a publicly available resource (https://doi.org/10.6084/m9.figshare.9204998). This GWAS study included 175,226 persons of European ancestry, comprising 164,610 persons from the UKB aged 60-70 years and 10,616 persons from the Swedish

Please cite this article in press as: Jia et al., Plasma proteomic signature of frailty in 50,506 adults, Cell Metabolism (2026), https://doi.org/10.1016/j.cmet.2026.02.013

CellPress
OPEN ACCESS

TwinGene study aged 41-87 years.[19] To avoid potential sample overlap with the UKB-PPP discovery cohort, only GWAS summary statistics from the TwinGene study was used in the MR analyses.

MR analyses were performed using the TwoSampleMR R package. The Wald ratio method was used to obtain MR effect estimates for proteins with only one instrument, whereas the IVW method was used for proteins with more than one instrument. Statistical significance was defined as FDR-corrected $P < 0.05$. Steiger filtering was applied to assess the directionality of associations. Horizontal pleiotropy was evaluated using the MR-Egger intercept and the MR Pleiotropy RESidual Sum and Outlier (MR-PRESSO) global test, and heterogeneity among IVs was assessed using Cochran's *Q* statistics. Additional analyses (i.e., simple mode, weighted mode, weighted median, and MR-Egger) were also performed to assess the robustness of causal estimates.

Colocalization analyses

To evaluate whether the genetic association signals for protein levels and frailty arose from a shared causal variant, colocalization analyses were conducted using the coloc R package. Five posterior probability hypotheses were tested: 1) no shared causal variants for either trait (H0); 2) causal variant for gene expression only (H1); 3) causal variant for disease risk only (H2); 4) distinct causal variants for each trait (H3); and 5) a shared causal variant for both traits (H4). Analyses were performed within a ±250-kb window centered on each gene's coding region. Evidence for colocalization was considered strong if the posterior probability for shared causal variants (posterior probabilities for the H4 hypothesis [PPH4]) was ≥ 0.7.[72]

SMR analysis

SMR analyses were further conducted as a complementary approach to validate the causal associations using SMR software (SMR v1.3.1). The HEIDI test, using multiple SNPs in a region, was used to distinguish proteins that were associated with frailty owing to a shared genetic variant rather than genetic linkage.[73] A Bonferroni-corrected $P < 0.01$ (0.05/5) was considered statistically significant for SMR analyses, while the *P* of the HEIDI test > 0.05 indicated that the observed association was unlikely to be driven by linkage disequilibrium.